FINITE ELEMENT MODELLING OF DAMAGE PROCESSES IN ICE-STRUCTURE INTERACTION

JING XIAO, B.Eng.

Finite Element Modelling of Damage Processes in Ice-Structure Interaction

by

© Jing Xiao, B.Eng.

A thesis submitted to the School of Graduate Studies
in partial fulfillment of the requirements for the degree of
Master of Engineering

Faculty of Engineering and Applied Science
Memorial University of Newfoundland
August, 1991

St. John's Newfoundland Canada

ISBN 0-315-73349-7

Abstract

Two field programs were carried out on the Hobson's Choice Ice Island in April, 1989 and May, 1990 using different sizes of spherical and flat indenters. Several cores of multiyear field ice were recovered from the ice island and transported to Memorial University to conduct compressive tests in the laboratory. Both constant strain-rate tests and constant stress tests were performed with uniaxial stress to investigate the deformation of multiyear ice and calibrate the material constants for theoretical modelling.

The spherical indentation tests are modelled using an axisymmetrical finite element model. The ice damage process is related to the growing network of micro-cracks and the ice creep process is also enhanced by the existence of cracks. The damage model is developed in FORTRAN code and implemented as a user subroutine in the ABAQUS finite element analysis program. The analysis results show that most of the ice damage is close to the contact surface, and that the maximum damage occurs at the edge of the interface where shear stress is concentrated. This is in agreement with the test results. The model also provides good results on the total load versus time history.

Acknowledgements

I am very grateful to the faculty of Engineering and Applied Science that, in many ways, provided assistance in the completion of this project. Without their active collaboration and cooperation this project would have remained an unfulfilled dream. In particular, I am greatly indebted to Dr. Ian Jordaan, my thesis supervisor, who not only helped at every stage of the development, reading through all of the early drafts of the manuscript time and time again, but who also had a profound influence on my academic training through scholarship, and whose constructive comments and meticulous criticism have been a constant source of inspiration and encouragement during the writing of this thesis.

Special thanks go to Dr. Richard McKenna who not only provided me with much guidance as well as assistance during the process of completing this project, but who also introduced me to many relevant readings and materials.

I wish to especially thank my friends and colleagues, Sanjay Singh, Rick Meaney and Shawn Kenny for their constant encouragement, as well as sincere concerns, valuable suggestions and criticisms throughout my research. I also want to extend my gratitude to Mr. Barry Stone, whose concrete help and contribution in many of my laboratory experiments are gratefully acknowledged.

Finally, a special word of thanks goes to my wife, Yang Meng, for her help in designing the format. I want to acknowledge gratefully her keen eye for noting discrepancies, and her patience in typing and making changes and additions.

Contents

List of Figures

List of Tables

Nomenclature

σ_{ij}	stress tensor (MPa)
ϵ_{ij}	strain tensor
E	elastic modulus (MPa)
E_k	elastic stiffness in Kelvin unit
E_m	elastic stiffness in Maxwell unit
G	shear modulus (MPa)
K	bulk modulus (MPa)
ν	Poisson's ratio
t	time (s)
μ	viscosity coefficient (MPa·s)
μ_k	viscosity in Kelvin unit
μ_m	viscosity in Maxwell unit
C_{ijkl}	forth order compliance tensor
ϵ_{ij}^e	elastic strain components
ϵ_{ij}^d	delayed elastic strain components
ϵ_{ij}^c	secondary creep strain components
e_{ij}^e	elastic strain deviator
e_{ij}^d	delayed elastic strain deviator
e_{ij}^c	secondary creep strain deviator
e	equivalent strain
ϵ_v	volumetric strain
σ_v	volumetric stress (MPa)
s	von Mises stress (MPa)
s_{ij}	stress deviator (MPa)
σ_c	critical stress for crack nucleation (MPa)
d	average grain size (m)
a	one half of the crack length (m)
N	crack density

D_N	damage parameter
$\dot{N}_0$	damage constant
β	creep enhancement parameter
$\dot{\epsilon}_0^d$	delayed elastic strain reference rate
$\dot{\epsilon}_0^c$	secondary creep strain reference rate
δ_{ij}	delta function
m	damage exponent
n	creep exponent

Chapter 1

Introduction and Scope

Since early 1980s, increased exploration for conventional energy sources in the arctic and near-arctic offshore areas, has focused attention on the engineering problems of designing and building large structures in ice-covered waters. The interaction of ice with marine structures has been recognized as a major design consideration. There has been a great deal of effort in recent years, both experimentally and theoretically, to determine a reliable approach for the estimation of both global and local ice loads on offshore structures. These ice forces exerted on a structure may take many different modes, such as, crushing, fracturing, spalling, buckling, or the combinations of them. These are complex processes and involve several possible factors, such as, loading rate, ice type, temperature and the shape of interface.

Medium scale ice indentation tests were conducted on the Hobson's Choice Ice Island in April, 1989 (Frederking et al., 1990a, b) and in May, 1990, and also earlier in 1984, at Pond Inlet by Mobil Oil Canada (Geotech, 1985). In 1989 eleven tests were performed with three types of indenters, rigid spherical, flexible flat and rigid flat. There were six spherical indentation tests with a speed range from 0.3 mm/s to 90 mm/s. In all tests, ice crushing was observed in front of the indenter and

the thickness of the crushed layer was irregular. There was usually less cracking in the center area due to high confinement and more damage at the edge of the interface (in the present work, damage is related to the density of microcracks). Maximum pressures measured at the center were in the range of 10 to 20 MPa. Pressure melting has also been reported (Gagnon and Sinha, 1991).

Uniaxial tests have been performed on multiyear field ice which was recovered from the ice island. The comparison of the test results on both intact and predamaged ice show clear evidence of an enhancement of the creep strain due to crack and damage. The elastic modulus of the ice was calculated from the test results. An isotropic damage model, which utilizes a power-law relation between crack nucleation rate and stress, is used in the present work. This relationship is based on rate theory. Additionally, dilatation of ice under compression is modelled as a function of the ratio of volumetric stress to the equivalent von Mises stress. To verify this model, direct comparisons to the uniaxial tests have been performed.

Finite element analysis programs have been developed to simulate the spherical indentation tests at lower rates, with the ice damage model calibrated from uniaxial tests. The model predictions show good agreement with the test results on total load versus time histories and pressure distributions and progressions. The modelled damage distribution and progression can be utilized, to a certain degree, to characterize the layer of crushed ice. The calculation of ice viscosity is a simple approach, which is proposed to include the influence of confining pressure in further studies.

Finite element analysis with damage mechanics is a new and unique approach, in modelling ice behaviour under both uniaxial loading and medium scale indentation

testing conditions.

As outlined above, the scope of this work may be categorized as follows:

1. Literature review of recent theories on ice mechanics, including ice mechanical and damage models, as well as experimental observations on ice cracking behaviour.

2. Conducting uniaxial tests in the laboratory on the multiyear ice to calibrate the material constants for theoretical modelling; description of ice indentation tests carried out on Hobson's Choice Ice Island (1989) and some major observations.

3. Constitutive modelling of ice damage process, including creep enhancement due to the existence of cracks and damage; finite element implementation and model verification.

4. Finite element modelling of spherical indentation tests and comparison with the experimental results.

5. Conclusions and recommendations for further studies.

Chapter 2

Literature Review

Ice in nature is a polycrystalline material composed of a large number of single crystals usually in different orientations. Michel (1979) provided a detail description of the structure and classification of ice (see also Cammaert and Muggeridge (1988) on sea ice). Typically, there are two main kinds of polycrystalline ice found in nature:

1. Granular ice, which is randomly oriented polycrystalline ice, can be found in ice features; such as, glaciers, icebergs, lake ice and sea ice. The grain size is classified as fine to medium. In the laboratory, this type of ice can be obtained by freezing water seeded with full mould of randomly oriented fine ice crystals, and it can be treated as a statistically isotropic material.

2. Columnar ice is formed with the grains growing parallel to the heat flow and with c-axis perpendicular to the column length. This type of ice is referred to as S2 ice which can be found in lake, river and arctic sea ice. The mechanical properties of columnar ice are orthotropic, or more usually, transverse isotropic.

Ice is characterized as a viscoelastic material with its deformation response dependent upon the loading rate; it is also very brittle under high loading rate. A

spring-dashpot model, called Burger's model, is often used for polycrystalline ice. This model is a combination of a Kelvin unit and a Maxwell unit, as shown in Fig. 2.1.

The mechanical properties of ice can be divided into two parts (Sanderson,1988):

1. Continuum behaviour. This includes elastic and ductile creep deformation, which can be extended to include the uniformly distributed microcracking and damage processes.

2. Fracture behaviour. This includes crack propagation and brittle failure.

The continuum behaviour of granular ice is markedly similar to that of columnar ice, but with some differences due to orthotropy or anisotropy (Sinha, 1989a).

2.1 Elasticity of Ice

In engineering applications, the elasticity of granular ice is typically treated as isotropic and can be characterized by two constants, the elastic modulus, E, and Poisson's ratio, ν. When a constant load or stress σ is applied at time t_0 and released at time t_1, a strain versus time curve as shown schematically in Fig. 2.2 is produced. Following Hooke's law, the elastic strain of ice is given as

$$\epsilon_e = \frac{\sigma}{E}, \tag{2.1}$$

where the elastic modulus of ice is the stiffness of the main spring in the Maxwell unit and hence the elastic strain corresponds to the deformation of the main spring (see Fig. 2.1).

The elastic modulus and Poisson's ratio are dependent on the ice temperature and porosity. The variations of E and ν on temperature were given by Sinha (1989a)

for both granular and columnar ice. This work shows that temperature does not have a strong effect on these constants. The value of E changes from 9 GPa to 10.16 GPa and ν from 0.308 to 0.3605 in the temperature range -50 °C to 0 °C. There are two methods for determining the elastic modulus of ice: static and dynamic. The conventional static tests include uniaxial compression, uniaxial tension and beam bending. The two most common tests are uniaxial compression tests under either constant load (or stress) or constant displacement rate (or strain rate). The former test gives a strain versus time curve as shown in Fig. 2.2, and the elastic modulus $E = \sigma/\epsilon_e$, for t=0; the latter test gives a stress versus strain curve as shown in Fig. 2.3, and the elastic modulus $E = \frac{d\sigma}{d\epsilon}$, when ϵ=0. So the calculated value of elastic modulus is strongly dependent on the accuracy of the test. However, ice is not purely elastic, it creeps at all stresses with a time-dependent rate, so readings of the initial tangent modulus from a stress-strain curve will not be very accurate. Dynamic testing techniques are considered to be more accurate since they minimize the time-dependent effects. For polycrystalline ice of low porosity, the elastic modulus given by high frequency dynamic measurements is approximately 9 to 9.5 GPa in the temperature range -5 °C to -10 °C (Mellor, 1983). This is a standard range of values of elastic modulus for low porosity polycrystalline ice. The commonly accepted range for Poisson's ratio is 0.3 to 0.33.

The elastic modulus of sea ice has been investigated by Mellor (1983) based on previous research, which shows that elastic modulus of sea ice varies from 10 GPa (pure ice) to 1 GPa in the porosity range 0 to 0.3. Theoretical models which calculate the elastic modulus as a function of brine volume were also proposed by Weeks and Assur (1967), Schwarz and Weeks (1977).

2.2 Creep of Ice

A constant stress creep test on polycrystalline ice gives a conventional creep curve as shown in Fig. 2.4. The idealized creep curve can be divided into three phases: primary, secondary and tertiary creep. The role of each individual phase in creep deformation has not been fully understood. In general, the deformation of ice includes several kinds of processes or mechanisms, and the influence of each individual process or phase might be maximized or minimized depending on the type of ice, temperature and loading condition. Each of these three phases could dominate the creep strain under certain circumstances. Sinha (1978) developed a viscoelastic constitutive equation for columnar ice under uniaxial compression. The total strain ϵ is considered as the sum of three components as shown in Fig. 2.2, i.e.

$$\epsilon = \epsilon^e + \epsilon^d + \epsilon^c \tag{2.2}$$

where ϵ^e is the instantaneous elastic component; ϵ^d is the delayed elastic component, or recoverable primary creep, and ϵ^c is the permanent viscous component, or secondary creep strain. Sinha's model is limited to the first two phases of creep and does not address the tertiary creep phase.

Sinha (1978) gives an expression for delayed elastic strain under constant stress

$$\epsilon^d(t) = \frac{c_1 d_1}{d}\left(\frac{\sigma}{E}\right)^s [1 - \exp\{-(a_T t)^b\}], \tag{2.3}$$

where c_1, s, b and a_T are all constants depending on the temperature and the grain size, d; where $E = 9.5$ GPa; $c_1 = 9$, is a constant corresponding to the unit grain size d_1 ($d_1 = 0.001$); $s = 1$; $b = 0.34$; $a_T = 2.5 \times 10^{-4} s^{-1}$ ($T = 263K$). The delayed elastic strain corresponds to the deformation of the Kelvin unit in Fig. 2.1.

A nonlinear dashpot based Kelvin unit was proposed by Jordaan and McKenna (1988b) to model delayed elastic strain, in which the viscosity μ_k is a function of stress σ_d in the dashpot. The strain in the Kelvin unit is then

$$\epsilon^d(t) = \frac{\sigma}{E_k}[1 - \exp\{-\int_0^t \frac{E_k}{\mu_k(\sigma_d)}\, dt\}] \tag{2.4}$$

where E_k is the elastic modulus of the spring, and μ_k is the viscosity of the dashpot in the Kelvin unit. It was assumed that the dashpot follows a power-law relation with stress

$$\mu_k(\sigma_d) = \frac{1}{K_k\, \sigma_d^{n-1}} \tag{2.5}$$

where K_k is the viscosity parameter; n is a constant. Using the equation of equilibrium for the element of the Kelvin unit, i.e.

$$\frac{\dot{\sigma} - \dot{\sigma}_d}{E_k} = \frac{\sigma_d}{\mu_k(\sigma_d)}$$

then it is found

$$\mu_k = (n-1)E_k t + \mu_{k0}. \tag{2.6}$$

Substituting Eq. (2.6) into Eq. (2.4), the delayed elastic strain is then given by

$$\epsilon^d(t) = \frac{\sigma}{E_k}\{1 - [(n-1)\omega t + 1]^{1/(1-n)}\} \tag{2.7}$$

where, $\omega = E_k/\mu_{k0}$, μ_{k0} is the viscosity at time $t = 0$.

The secondary creep strain describes the effect of the viscous flow and dislocation movement within the grains, and appears to be independent of the grain size (Cole, 1986). This creep strain corresponds to the creep deformation in the

dashpot of the Maxwell unit (see Fig. 2.1). For polycrystalline ice under uniaxial compression or tension, a power-law relation of strain rate and stress was suggested by Glen (1955) of the form

$$\dot{\epsilon}^c = A\sigma^n$$

where n is a constant and A is a function of temperature in the form

$$A = B \exp\left(\frac{-Q}{RT}\right), \tag{2.8}$$

where $R = 8.314$ J mol^{-1} K^{-1}, is the universal gas constant; T is the temperature in degrees Kelvin; Q is the activation energy and B is a material constant, both Q and B are dependent of the ice type.

In Sinha's expression for columnar ice, the creep strain rate was given by a similar relationship:

$$\dot{\epsilon}^c = \dot{\epsilon}_0^c \left(\frac{\sigma}{\sigma_0}\right)^n, \tag{2.9}$$

where $n = 3$, and $\dot{\epsilon}_0^c = 1.76 \times 10^{-7} s^{-1}$ $(T = 263K)$, is the viscous strain rate for unit stress σ_0, $(\sigma_0 = 1$ MPa).

The tertiary creep was considered due to the effect of microcracking (Gold, 1970), but it was found that cracking is not essential for the occurrence of tertiary creep in polycrystalline ice, even during the transition from primary to tertiary creep (Mellor and Cole, 1982). The real process is not well understood. In this study, secondary creep includes enhancement associated with the current level of crack density. This crack-enhanced creep is used to model the permanent creep strain.

The viscosity of sea ice is different from that of pure ice, since sea ice contains many air bubbles, brine pockets and impurities which causes local stress discontinuities and concentrations; hence, sea ice is softened and has lower viscosity (Pounder, 1965), (Wang, 1979a, b, 1981), (Weeks and Assur, 1967). A rationalized creep rate expression of sea ice was given by Sanderson (1988) as

$$\dot{\epsilon}^c = A'\sigma^3,$$

where

$$A' = B\exp\left(\frac{-Q}{RT}\right)\frac{1}{(1-\sqrt{\nu_b/\nu_0})^3}, \tag{2.10}$$

and ν_b is brine volume or porosity of the ice and ν_0 is a normalizing constant. Substituting Eq. (2.8) into Eq. (2.10), it is found that

$$A' = A\frac{1}{(1-\sqrt{\nu_b/\nu_0})^3}. \tag{2.11}$$

For multiaxial stress states, the elastic response of ice can be written as

$$\dot{\epsilon}^e_{ij} = C_{ijkl}\,\sigma_{ij}. \tag{2.12}$$

where C_{ijkl} is the fourth order compliance tensor; σ_{ij} is the second order stress tensor.

The delayed elastic strain rate, or recoverable creep strain rate was generalized by Ohno et al. (1985) to multiaxial stress states in the form

$$\dot{\epsilon}^d_{ij} = a[(3/2)K\,s^{b-1}\,s_{ij} - \epsilon^d_{ij}], \tag{2.13}$$

where a, K and b are material constants, which are possibly functions of strain and stress; s is the von Mises equivalent stress and s_{ij} is the deviatoric stress. If $b = 1$, the dashpot in the Kelvin unit is linear and the above equation becomes

$$\dot{\epsilon}^d_{ij} = a[\frac{3}{2} K s_{ij} - \epsilon^d_{ij}]. \tag{2.14}$$

This equation was adopted by Karr and Choi (1989).

The generalization of the secondary creep strain rate for incompressible behaviour of ice was given by Ashby and Duval (1985) as

$$\dot{\epsilon}^c_{ij} = \frac{3}{2} K' s^{n-1} s_{ij} \tag{2.15}$$

where K' is a viscosity constant. So the total strain rate of ice is then

$$\dot{\epsilon}_{ij} = \dot{\epsilon}^e_{ij} + \dot{\epsilon}^d_{ij} + \dot{\epsilon}^c_{ij} \tag{2.16}$$

where ϵ_{ij} is the second order strain tensor.

2.3 Cracking of Ice

Crack nucleation in ice is a complex process associated with the transition from ductile to brittle behavior. The mechanism of nucleation depends on the load level and loading rate. Gold (1972) first described the failure of columnar-grained ice in terms of microcracking during compressive creep tests, with special attention to the crack initiation time, strain and crack density development. Based on statistical analysis, two types of crack distributions were found. Strain-dependent crack distributions were proposed to be the result of a dislocation pileup mechanism. Strain-independent crack distributions appeared to be related to the elastic anisotropy which causes stress concentrations at grain boundaries.

For fracture of ice in tension, the applied load must be sufficient to nucleate microcracks, and the load must be increased until the crack begins to propagate. Crack nucleation is likely to be associated with critical tensile strain (Seng-Kiong

and Shyam Sunder, 1985) or critical delayed elastic strain as proposed by Sinha (1982).

For ice of grain size less than 1 mm, nucleation of cracks may occur at a stress of about 1 to 1.2 MPa and the propagation stress is about 1.2 to 2 MPa. From test data obtained at strain rates $10^{-6}s^{-1}$ to $10^{-3}s^{-1}$ by Schulson et al. (1984, 1989), Schulson (1987, 1989), and Currier et al. (1982), tensile crack nucleation occurs at a critical stress which can be expressed as

$$\sigma_N = \sigma_0 + k\, d^{-1/2} \tag{2.17}$$

where σ_0 is 0.6 MPa and k is 0.02 MPa $m^{1/2}$ and d is the grain size. The criterion for tensile crack propagation is given by

$$\sigma_P = \frac{Y\, K_{IC}}{(\pi a)^{1/2}} \tag{2.18}$$

where K_{IC} is the critical stress intensity factor for mode I loading, a is half of the crack length and Y is a geometrical parameter. Tensile cracks and fracture surfaces are always perpendicular to the tensile stress axis.

In compression, the crack nucleation process is more complicated and highly rate sensitive. Seng-Kiong and Shyam Sunder (1985), Hallam (1986) proposed that crack nucleation occurs when the associated lateral tensile strain induced by the Poisson expansion reaches a critical value. The required compressive nucleation stress should be about 3 times higher than that for tension.

Sinha (1984) used the test results of Gold (1972) to relate crack nucleation to a critical delayed elastic strain associated with grain boundary sliding, i.e., the delayed elastic strain ϵ^d given in Eq. (2.3) is equal to the strain induced by the grain

boundary sliding ϵ_{gbs}, and when ϵ_{gbs} reaches a critical value ϵ'_{gbs}, crack nucleation occurs. The critical value of grain boundary sliding ϵ'_{gbs} is related to the critical stress needed to produce a crack at the end of a sliding interface.

The dislocation pileup mechanism was adopted by Schulson et al. (1984) , Cole (1986) and Kalifa et al. (1989). This mechanism is based on the concept that dislocation pileup at grain boundaries may provide a high stress concentration which can induce crack nucleation when the stress reaches a critical level.

More tests were carried out recently by Sinha (1988) on columnar ice, Hallam et al. (1987) on granular ice at constant load, and by Cole (1986) on granular ice at constant strain rates. Kalifa et al. (1989) performed a series of triaxial compression tests with strain rates varying between $2.5 \times 10^{-5} s^{-1}$ and $10^{-3} s^{-1}$ and confining pressure ranging from 0 MPa to 10 MPa.

From their work some conclusions can be summarized:

(1) Cracks usually start from the grain boundaries where high stress concentrations exist and are arrested at grain boundaries. Crack nucleation occurs at the larger grains first. The plane of cracks has a strong tendency to be parallel to the axis of compressive stress.

(2) For the constant stress tests (Cole, 1986), the crack density increases with grain size and stress, and the cracking rate decreases as the crack density approaches one crack per grain.

(3) The number of intergranular (between the grains) and intragranular (within the grains) cracks are about the same, but cracks are preferentially intergranular at high strain rates.

(4) The average crack size is about 0.65 times the average grain size, and the

maximum crack size is typically 2 to 3 times the average grain size. The crack size is not affected by the stress. The grain size was calculated, according to Cole (1986), using $d = (6/\pi N)^{1/2}$, where N is the number of gains per unit area. It was found that the peak stress decreases with increasing grain size.

(5) Although the final crack density is very high, the microcracks do not appear to interact; that is, the nucleation of one crack does not trigger the other crack nearby.

(6) No "wing cracks" were observed by Cole (1986) and Kalifa et al (1989). On the other hand, a few wing cracks were observed by Hallam et al. (1987) and Schulson (1987), but damage in ice is mainly due to the nucleation of new grain-sized cracks, rather than the propagation of those which have already nucleated.

(7) According to Kalifa et al. (1989), the stress and strain levels for crack nucleation increased with the confining pressure, and so did the standard deviation of the distribution of crack orientation. The size of cracks did not change with pressure and the strain rate has no significant effect on crack nucleation. An equation of the critical stress at the first cracks was given as

$$\sigma_1 - \sigma_3 = -2.47 + 0.4\,\sigma_3 \tag{2.19}$$

where σ_1 is axial stress and σ_3 is confining stress. Both σ_1 and σ_3 are negative in compression.

There are four stages in the failure process of ice during compression experiments of strain rate at $10^{-3}s^{-1}$ (Cole, 1989):

(1) In the first stage, stress-strain relation is basically elastic but with slightly nonlinear behavior and no visible microcracking observed.

(2) Microcracks begin to nucleate in the second stage with stress between 3.29 MPa to 3.95 MPa. The crack density increased very quickly with increasing stresses up to 5.65 MPa.

(3) Crack nucleation stopped, the increasing stress causes no more visible microstructural damage and the existing cracks appear stable.

(4) The final stage is the specimen completely damaged with possibly sudden brittle failure.

In fact, only when the strain rate is relatively high, about $10^{-3}\,s^{-1}$, does the ice become brittle and complete fracture failure occurs. In this case cracks extend to the free surface or cracks interact to form a larger crack or shear fracture surface. If the loading rate is low, the stress-strain curve eventually reaches a plateau and ice creeps without sudden failure.

The elastic anisotropy mechanism has also been applied to ice by Cole (1988) and Shyam Sunder and Wu (1990). Their recent work showed that elastic anisotropy of the ice lattice is an effective source of stress concentration and can be taken as an alternative for crack nucleation when deformation rate is too high to allow dislocations to pileup. These models gave good agreement with test results.

Microcracking and fracture of ice is very common in ice indentation and there is much work on ice interacting with flat, cylindrical and spherical indenters. As addressed in the work of Jordaan and Timco (1988), Timco (1986), Tomin et al. (1986) and Jordaan and McKenna (1988a), when an ice sheet interacts with a flat indenter, a layer of crushed ice is formed in front of the indenter and the microcracks are developed along the maximum shear stress, as shown in Fig. 2.5a. The ice is idealized into three zones, as shown in Fig. 2.5b, undamaged virgin ice;

partly damaged ice with relatively high density of cracks and reduced stiffness; and crushed ice which eventually will be extruded out but this ice can carry compressive loads due to its frictional properties, i.e. the compressive strength of crushed ice is not zero.

Several different failure modes of an ice sheet were observed (Timco 1986) depending on the loading rate and the ratio of the indenter width to ice thickness. Generally, at low speed, there is mainly crushing and microcracking in the ice with some short cracks less than a few centimeters in length (Fig. 2.5). At high speed, there is crushing and spalling right in front of the indenter, but the failure of ice is mainly due to the occurrence of the radial and circumferential cracks and maybe buckling (Fig. 2.6a). In some cases there are mainly 45° - 60° radial cracks extending from the corners and the cracks would be a couple of meters long (Fig. 2.6b). More tests have been carried out recently in the ice tank in the Institute for Marine Dynamics, Canada, which provides similar evidence of ice cracking in interaction (Finn, 1991). In the case of the cylindrical indention, crushing, microcracking, radial and circumferential cracks can also be observed similarly to the flat indention (Hallam, 1986). A possible crushing and damage mode of the spherical indentation tests, as discussed in the work of Jordaan and McKenna (1988a), is illustrated in Fig. 2.7. A layer of crushed ice is under the indenter and the ice beyond the crushed zone is partly cracked. The density of the crushed ice is less than the intact ice. Radial cracks could also form and reach the surface, so large flakes would spall away. More details of this kind of tests will be discussed later.

2.4 Damage Mechanics and Damage of Ice

The deformation process of engineering materials under loading often results in changing the structure of the material. This change, to a large degree, will depend on the combined effects of geometry, loading, and the most important, the growth of micro-defects in the structure. The accumulation of micro-defects is often termed "the process of damage" which is always associated with the change of the mechanical behavior of the material and the dissipation of strain energy. Most of the early work of damage mechanics was based on the original idea that the damage of a structure can be measured by a scalar factor (Kachanov, 1958), which is equal to the ratio of the area of voids and the whole cross section, or the density of microcracks and voids which would permanently affect either the elastic modulus, E or shear modulus, G. This was the guideline for most of the early work. The importance of this kind of damage models is the establishment of a rational damage law which defines the rate of damage accumulation in terms of the current values of state variables and internal variables.

Based on Kachanov's model (1986), a body with an overall section area A_0 and fractured (damaged) area A, is shown in Fig. 2.8. In the case of uniaxial loading P without damage, stress in the body is given as

$$\sigma = \frac{P}{A_0}. \tag{2.20}$$

With isotropic damage, the damage variable D can be defined as

$$D = \frac{A}{A_0};\ 0 \leq D \leq 1 \tag{2.21}$$

and the effective stress σ_a is introduced as

$$\sigma_a = \frac{P}{A_0 - A} = \frac{P}{A_0(1-D)} = \frac{\sigma}{1-D}. \tag{2.22}$$

It is assumed that the strain response of the body is modified by damage only through the effective stress, so the stress-strain relation of the damaged material is

$$\varepsilon = \frac{\sigma_a}{E_0} = \frac{\sigma}{E_0(1-D)} = \frac{\sigma}{E} \tag{2.23}$$

where E_0 is the elastic modulus of virgin material and $E = E_0(1-D)$ can be called the "effective" modulus. So the behaviour of damaged material can be considered to be equivalent to the behaviour of undamaged material, provided that the original elastic modulus E_0 is replaced by

$$E = E_0(1-D). \tag{2.24}$$

The evolution of damage generally relates the present strain, stress and damage. The kinetic or evolutional equation can be introduced in the general form

$$D = f(e, \dot{e}, \sigma, \dot{\sigma}, D, \cdots, \dot{D}) \tag{2.25}$$

where e, σ and D are strain, stress and damage respectively.

A continuum damage model was proposed by Resende and Martin (1983, 1984) for rock-like materials which defines the elastic strain-stress relation of the material as

$$s = G_0(1-D)e^e \tag{2.26}$$

and

$$\dot{e} = \dot{e}^e + \dot{e}^p \tag{2.27}$$

where s is the stress invariant; G_0 is the initial shear modulus; D is the damage measurement; e is the total shear strain invariant, and e^e and e^p are the elastic and damage part of e, respectively. So the rate form of Eq. (2.24) was given as

$$\dot{s} = G_0(1 - D)\dot{e}^e - G_0 e^e \dot{D}; \text{ for loading } (\dot{D} > 0), \text{ and} \tag{2.28}$$

$$\dot{s} = G_0(1 - D)\dot{e}^e; \text{ for unloading } (\dot{D} = 0). \tag{2.29}$$

The damage evolution law was defined as

$$\dot{D} = \dot{D}(\dot{e}, e, \sigma_m, \dot{\epsilon}_v, \epsilon_v) = A(e, \sigma_m)\dot{e} + B(\epsilon_v)\dot{\epsilon}_v \tag{2.30}$$

where A and B are material constants and dependent on loading situation. The invariant volumetric strain rate $\dot{\epsilon}_v$ was also assumed as

$$\dot{\epsilon}_v = \dot{\epsilon}_v^e + \dot{\epsilon}_v^p \tag{2.31}$$

where $\dot{\epsilon}_v^e$ and $\dot{\epsilon}_v^p$ are the elastic component and inelastic damage component respectively. They are also functions of strain, stress and damage. See the references for details. Other references on damage mechanics include Krajcinovic (1983); Krajcinnovic and Fonseka (1981); Leckie (1978); Schapery (1981, 1984 and 1988).

Damage mechanics has been introduced to ice by Cormeau et al.(1986), McKenna et al. (1989), Jordaan and McKenna (1988), Karr (1985), Karr and Choi (1989), Sjölind (1987), etc. An isotropic damage model with a single scalar damage measure has been developed in some papers. Some of the recent work has focused on the relation of the extent of damage and the growing network of microcracks which is often assumed to be uniformly (isotropically) distributed and randomly oriented.

As described in the previous section, Sinha's model predicts crack nucleation when $\epsilon_{gbs} \geq \epsilon'_{gbs}$, and the formation of subsequent cracks was given in the form (Sinha, 1984, 1988, 1989b)

$$N = N_c[\psi \exp(\bar{x} - x_c) - 1] \tag{2.32}$$

where N_c is the crack density for the first cracks; ψ is a constant; $\bar{x}$ is the average grain boundary sliding (gbs) displacement; x_c is critical (gbs) displacement.

Creep strain rate was also found to be influenced by the formation of cracks. Following Weertman (1969), the enhancement of cracks on creep was given as (Sinha, 1988,1989b)

$$\dot{\epsilon^c} = \dot{\epsilon_0^c}(1 + 2\pi N a^2 n^{1/2})(\sigma/\sigma_0)^n;\ a^2 N \ll 1 \tag{2.33}$$

where N is the number of cracks per unit area and a is half of the crack length.

A rate expression of crack formation was also proposed by McKenna et al. (1989, 1990), Jordaan and McKenna (1989) based on rate theory in the form

$$\dot{N} = \dot{N}_c[\exp\left(\frac{\sigma - \sigma_c}{\sigma_0}\right) - 1], \tag{2.34}$$

and also

$$\dot{N} = \dot{N}_c\left(\frac{\sigma - \sigma_c}{\sigma_0}\right)^m; \tag{2.35}$$

where $\dot{N} = 0$, if $\sigma \leq \sigma_c$, σ_c is the critical stress, σ_0 is a constant(units of stress) and $\dot{N}_c$ is a reference rate. The isotropic damage parameter D_N, after Budiansky and O'Connell (1976), was defined as

$$D_N = a^3 N \tag{2.36}$$

where a is the same as above and N is the density of cracks m^{-3}.

When the crack density is high, the effect of cracks on the creep rate was estimated, based on the work of Weertman (1969), by introducing an exponential form

$$\dot{\epsilon} = \dot{\epsilon}_0 \exp(\beta N) \tag{2.37}$$

where β is a constant.

Some specially designed uniaxial tests were conducted on both intact and predamaged ice to investigate the influence of the presence of cracks on the deformation of ice, Stone et al. (1989), Jordaan and McKenna (1989) and Jordaan et al. (1990a, b). These tests were also used to verify the theoretical damage model and will be discussed in more detail later.

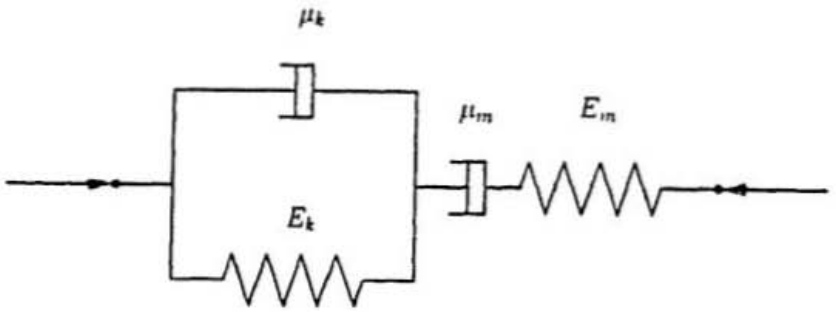

Kelvin unit Maxwell unit

Figure 2.1: Burgers Body; E and μ are elastic modulus and viscosity coefficient, respectively.

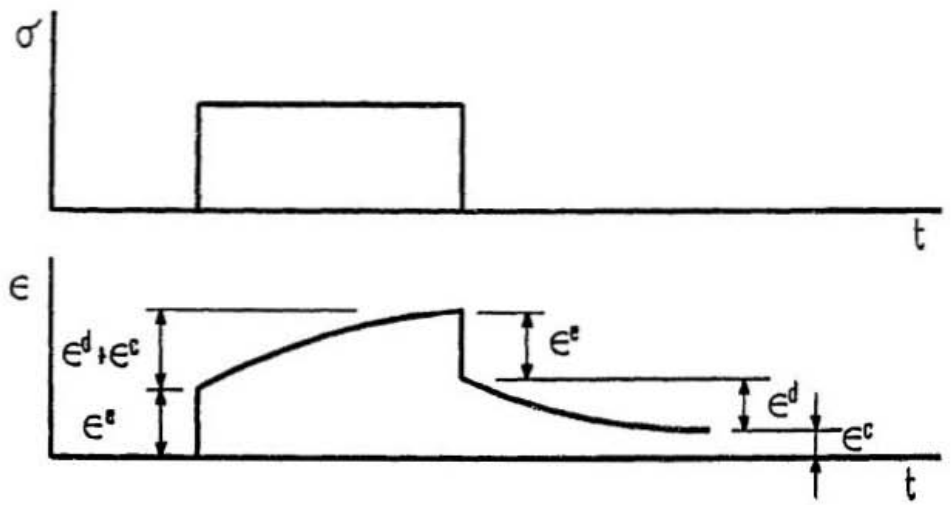

Figure 2.2: Applied stress history and strain response of constant stress test.

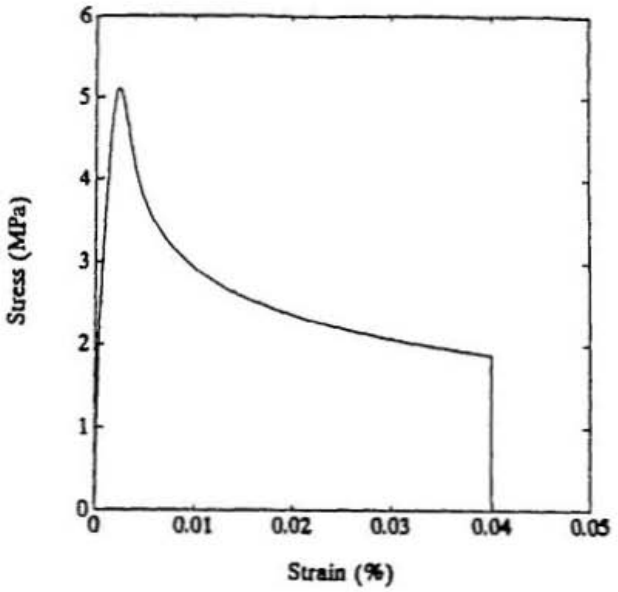

Figure 2.3: Stress-strain curve of constant strain rate test.

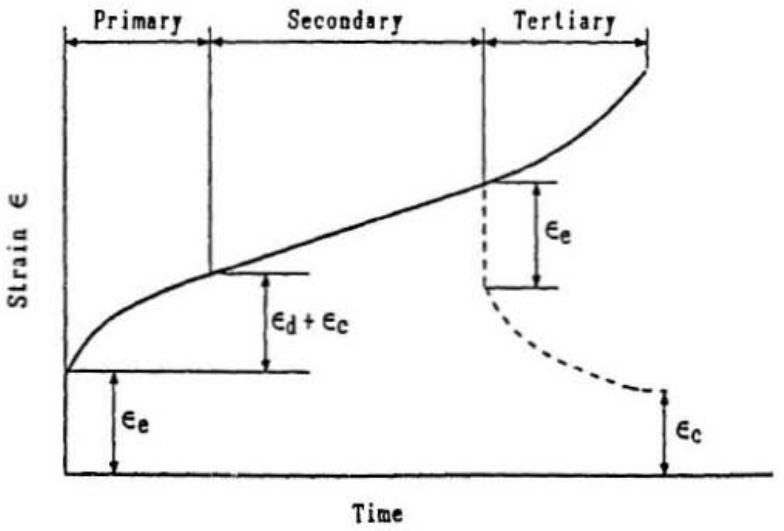

Figure 2.4: The three phases of creep test: (I) primary; (II) secondary; (III) tertiary.

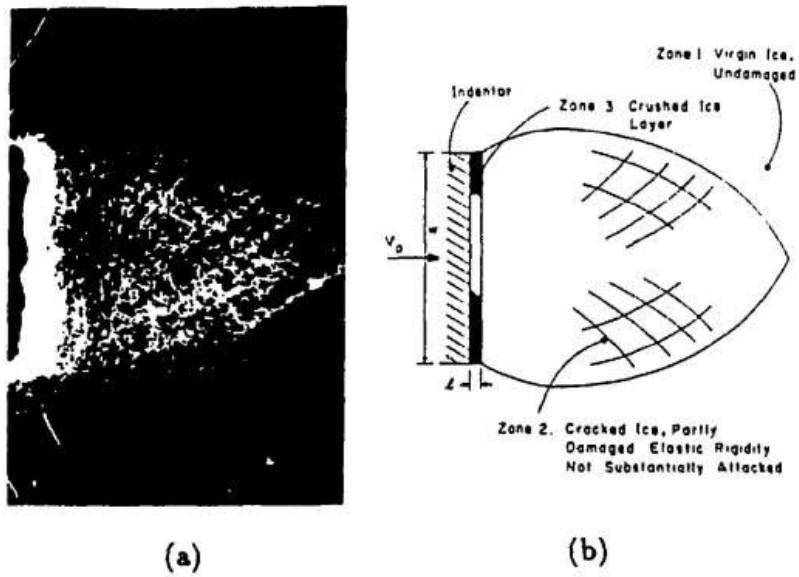

Figure 2.5: Idealization of ice sheet; plan view of (a) photographic representation showing progress of damage, and (b) idealization into three zones (Jordaan and Timco, 1988).

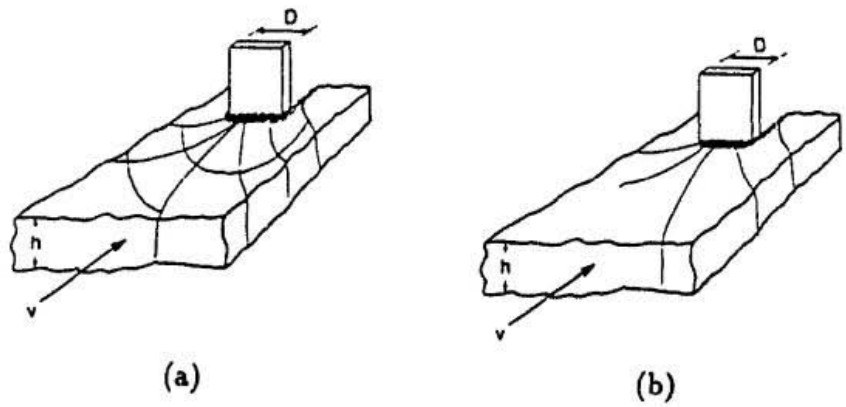

Figure 2.6: The failure modes observed in the ice sheet indentation tests: (a) Crushing with radial and circumferential cracking; (b) Crushing with radial cracking (Timco, 1986).

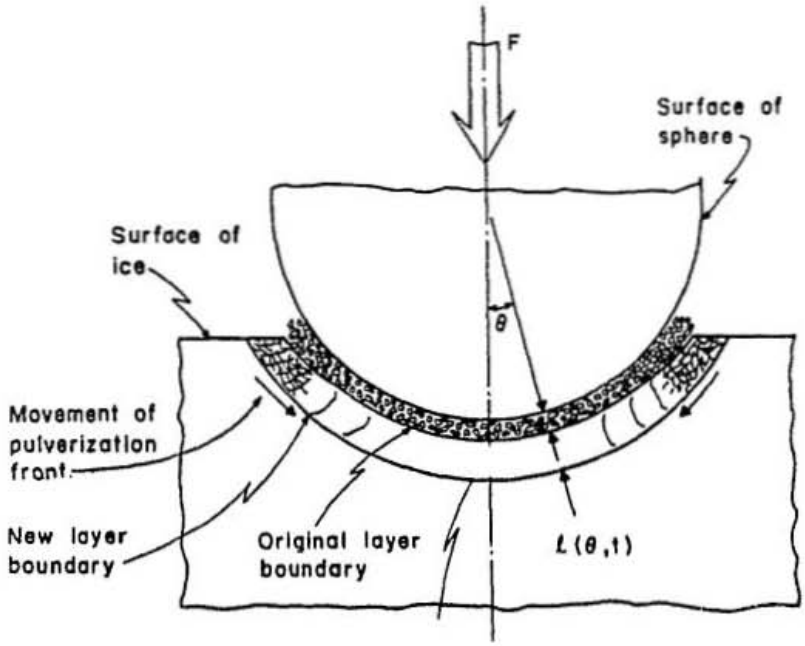

Figure 2.7: Possible mode of pulverization ahead of spherical indenter (Jordaan and McKenna, 1988a).

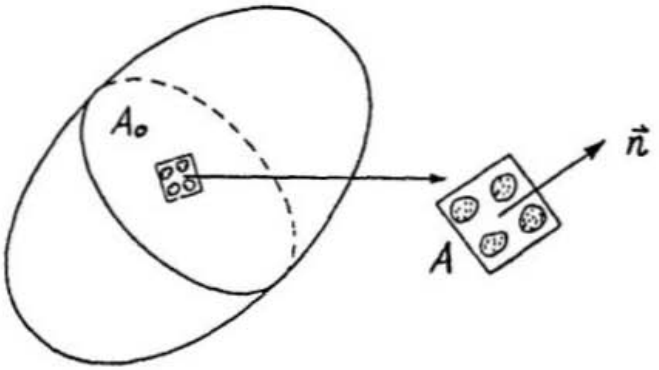

Figure 2.8: A body with an overall section area of A_0 and a damaged area of A.

Chapter 3

Experimentation

In April, 1989 and May, 1990, two field programs were carried out on Hobson's Choice Ice Island Research Station by Memorial University, the National Research Council of Canada (NRC), Canadian Coast Guard (CCG) and Sandwell Swan Wooster (SSW). A hydraulic indentation system was utilized with different sizes of spherical and flat indenters. The ice island is a 2.5 kilometer wide, 8 kilometer long, 45 meter thick floating block of ice that broke away from the Ward Hunt Ice Shelf, Ellesmere Island, in 1982. It is primarily composed of freshwater shelf ice, with a large amount of thick, up to 10 meters, multiyear ice surrounding the shelf ice core. The test site was in the area of multiyear ice (Kennedy, 1990; Frederking et al., 1990a, b). These programs were designed to determine an accurate and reliable methodology for the prediction of ice forces on offshore structures.

Several cores of multiyear field ice were recovered from the ice island and transported to Memorial University for compression testing in the laboratory. These tests were designed to investigate the deformation of multiyear ice, and to obtain the relevant material constants for theoretical modelling. The influence of cracks and damage on the creep response was investigated. As previously mentioned, sim-

ilar tests on freshwater ice were carried out by Stone et al. (1989), Jordaan and McKenna (1989) and Jordaan et al. (1990a, b).

3.1 Uniaxial Tests

3.1.1 Specimem Preparation

The block of ice-island ice was cut with a band saw into the shape of rectangular prism on the order of 75 × 75 × 200 mm^3. Cylindrical samples of desired diameter were machined from the rectangular samples on a lathe. Then the cylindrical samples were held on a precision V-block jig with its axis parallel to the longitudinal axis of the lathe and perpendicular to the cross head so that the sample could be cut to the desired size with two ends parallel and perpendicular to the axis of the cylinder. The final specimens were 54±0.05 mm in diameter and 135±0.25 mm in length. The sizes of the specimens were determined by the setup of the test system. The specimens were stored in a freezer at a temperature of -30°C until the test.

As reported by Frederking et al., (1990a) and Sinha (1990), the structure of the ice was basically frazil with a small portion of columnar ice, and comprised a significant number of air bubbles and brine pockets. The percentage of air pocket volume was around 2 to 5%. The grain size was about 2 to 7 mm. The salinity of the ice varied from 0 to 0.4% depending on the location, and the density was about 0.875 to 0.886 g/cm^3. Some photographs of the specimens, before and after the testing, are shown in Fig. 3.1. It was found that there were about 4 – 8 big bubbles, on the order of 2.5 to 5 mm in each specimen, plus groups of bubbles with the size of 1 to 2 mm and randomly distributed small bubbles with the size of 0.3 to 0.7 mm.

3.1.2 Test Setup

A MTS Systems Corporation Model 905 Structure Testing System was used for all tests. Two LVDT's were mounted directly on the specimen as shown in Fig. 3.2, over a gauge length of approximately 85 mm. The two LVDT outputs were averaged to provide the in-situ measure of axial strain as well as a closed-loop feedback control signal to the MTS servo-valve. Lateral strain was also measured on the first two tests to try to find evidences of dilatation during the deformation. For this purpose, two LVDT's were mounted on the two sides of the specimen and approximately on a line as shown in Fig. 3.3, but the results were not very satisfactory due to the irregular deformation of the specimen in the lateral direction, which is evident in Fig. 3.1.

Several hours before each test, the specimen was placed in the cold room to allow temperature equalization. During the test, the temperatures at the top and bottom of the specimen were measured. The temperature at the bottom was usually slightly higher than that at the top. This was attributed to the hydraulic fluid being supplied from outside the cold room. A maximum bottom temperature of -9.6°C was measured for -10°C tests.

All the test data including load, stroke, displacement and time, were recorded on a microcomputer via a multifunction data acquisition board. According to Stone et al. (1989), an acquisition rate of 75 sample/sec/channel was found to be adequate for loading and unloading phases of the tests at strain rates of $10^{-4}s^{-1}$ to $10^{-5}s^{-1}$. For the higher strain rate of $10^{-3}s^{-1}$, an acquisition rate of 175 samples/sec/channel was recommended. Between each unloading and loading, i.e., during the period of relaxation, where the deformation rate is very low, the acqui-

sition rate is set to 10 - 100 times lower than that on loading, so that more storage space in the computer can be saved. The data acquisition rate for the creep tests was 245 samples/sec/channel during the loading. The acquisition board provides a measurement accuracy and resolution of ±0.02% in the range of ±10V. Load and stroke were also plotted by an X-Y plotter during the tests.

3.1.3 Results and Discussion

As listed in Table 4.1, three uniaxial constant strain rate tests and five constant load tests were carried out on the multiyear ice described in section 3.1.1. At the temperature of -10°C, test No. 1 was a constant strain-rate test subjected to a loading rate of $5 \times 10^{-5} s^{-1}$ to a maximum strain of 2% as shown in Fig. 3.4. Test No. 2 was similar but had two loadings with different rates. The specimen was first loaded at a strain rate of $5 \times 10^{-5} s^{-1}$ to a strain of 2%, followed by unloading and about 100 seconds of relaxation, followed again by reloading at a strain rate of $2.5 \times 10^{-5} s^{-1}$ to a total strain of 4%, as shown in Fig. 3.5. Test No. 3, conducted on an intact ice specimen, was a constant stress creep test, which was a series of creep tests. Each creep test consisted of a 20 second load pulse followed by a 10 minute relaxation period, followed again by reloading, and so on (see Fig. 3.6). The reason for loading only 20 seconds is that these tests were designed to investigate the short-time responses of ice, such as, elastic and delayed elastic strain components. Test No. 4 was a creep test conducted on a predamaged specimen. The specimen was predamaged by subjecting to a constant strain rate loading of $10^{-4} s^{-1}$ to a strain of 2% as shown in Fig. 3.7. At the temperature of -20°C, a creep test, No. 5, on an intact specimen was carried out with the same loadings

Table 3.1: List of the Test Series

No.	test type	strain rate or stress	ice type	temp. °C	remarks
1	constant strain rate (C.S.R.)	$5 \times 10^{-5} s^{-1}$ (see Fig. 3.4)	intact ice	-10°C	
2	constant strain rate	$5 \times 10^{-5} s^{-1}$ & $2.5 \times 10^{-5} s^{-1}$ (see Fig. 3.5)	intact ice	-10°C	sample was reloaded at strain of 2%
3	constant stress (C.S.)	0.25 MPa — 1.5 MPa (see Fig. 3.6)	intact ice	-10°C	
4	constant stress	0.25 MPa — 2.0 MPa (see Fig. 3.7)	p.d.† ice	-10°C	† predamaged; sample was predamaged under C.S.R. to 2% strain
5	constant stress	0.25 MPa — 2.0 MPa (see Fig. 3.8)	intact ice	-20°C	
6	constant stress	0.25 MPa — 2.0 MPa (see Fig. 3.9)	p.d. ice	-20°C	sample was predamaged under C.S.R. to 2% strain
7	constant stress	0.25 MPa — 2.0 MPa (see Fig. 3.10)	p.d. ice	-20°C	sample was predamaged under C.S.R. to 2% strain
8	constant strain rate	$5 \times 10^{-4} s^{-1}$ & $10^{-3} s^{-1}$ (see Fig. 3.11)	intact ice	-20°C	sample was reloaded at strain of 2% strain

as that of test No. 3 (Fig. 3.8). Test No. 6 and No. 7 were two creep tests on predamaged specimens, i.e., the ice was loaded to a total strain of 2% at constant strain rate of $10^{-4} s^{-1}$, as shown in Fig. 3.9 and Fig. 3.10, respectively. Test No. 8 was a constant strain rate test, as shown in Fig. 3.11, to a strain of 2% with a strain rate of $5 \times 10^{-4} s^{-1}$, and reloaded again to a strain of 4% with a strain rate of $10^{-3} s^{-1}$.

Fig. 3.12 shows the stress-strain curves of some constant strain-rate tests on

both freshwater and multiyear ice. Based on the unloadings of the tests on both types of ice, it was found that the recoverable strain, i.e. elastic strain plus delayed elastic strain, was less than 10% of the total strain. When the total strain is more than 2%, the stress reaches a plateau. The recoverable strain $\epsilon^e + \epsilon^d$ from the test of freshwater ice is only 2.05×10^{-3}, 1.82×10^{-3} and 2.84×10^{-3} upon first, second and third unloading, respectively. Notice that the first value is larger than the second, because the stress is higher at first unloading. The ice specimen was not totally relaxed during the first two unloadings; the relaxation periods were both about 10 minutes. The specimen relaxed for about one hour after the third unloading, therefore the third value of recoverable strain is the largest. But the secondary or permanent creep strain is still the predominant strain component. The ratios of recoverable strain to total strain are 10.5%, 5.2% and 5.5% for the three unloadings. This was also found in the tests of multiyear field ice.

Comparing the constant strain rate tests of multiyear ice to freshwater ice (Fig. 3.12) shows that the peak stresses of the multiyear ice are much lower. One reason for the lower strength must be the defects, such as the air pockets, in the multiyear ice. These defects can be considered as damage, which would significantly soften the ice. Another reason is that the structure of the multiyear ice is a combination of frazil and columnar ice with the grain size ranging from 2 mm to 7 mm. The laboratory-made freshwater ice is granular ice with a grain size of 3 mm. It is expected that the two kinds of ice would have different responses under the same loading. The multiyear ice, as addressed in the previous chapter, must have a lower viscosity due to defects and crystal structure. As shown in Fig. 3.12, the stresses start to build up almost linearly with strains and all the curves are close,

which means that the elastic modulus of the two types of ice have similar values, since most of the total strain is elastic strain at the beginning of loading (Sinha 1981). In the strain range of 0.1% to 0.5%, there is a significant difference in the stresses. The peak stress of the freshwater ice is almost double that of the multiyear ice. Assuming that the stress increases linearly to the peak stress, it is possible to estimate the portion of each strain component at the peak stress. i.e.

$$\epsilon^e = \sigma/E$$

$$\epsilon^c = \int_0^{t_p} \dot{\epsilon}_0^c \sigma^n \, dt$$

$$\epsilon^d = \epsilon - \epsilon^e - \epsilon^c.$$

Here σ is assumed to be

$$\sigma = \frac{\sigma_p}{t_p} t$$

where σ_p is the peak stress at time t_p. So it is found that

$$\epsilon^c = (1/4)\dot{\epsilon}_0^c \sigma_p^3 t_p$$

where $n = 3$ is assumed. Here the peak stresses are 5.7 MPa and 3 MPa for freshwater and multiyear ice, respectively, and t_p is 27.9 seconds. Assuming the two types of ice have the same elastic modulus, the viscosity parameter of freshwater ice is 1.76×10^{-7}(Sinha, 1981), and the estimation of porosity of the multiyear ice is about 5%. With Eq. (2.11), the viscosity parameter is calculated to be about 2.05×10^{-6}. The strain components at peak stress are listed in Table 4.2. So, for freshwater ice at peak stress, more than half of the total strain is elastic, but for multiyear ice, the delayed elastic strain is the largest component, and both ϵ^d

Table 3.2: List of Strain Components

	$\epsilon \times 10^{-3}$	$\epsilon^e \times 10^{-3}$	$\epsilon^d \times 10^{-3}$	$\epsilon^c \times 10^{-3}$	$\frac{\epsilon^e}{\epsilon}\%$	$\frac{\epsilon^d}{\epsilon}\%$	$\frac{\epsilon^c}{\epsilon}\%$
freshwater ice	1.395	0.788	0.383	0.224	56.5%	27.5%	16%
multiyear ice	1.395	0.417	0.591	0.387	30%	42.4 %	27.6 %

and ϵ^c are larger than that of freshwater ice. So it is concluded that the multiyear ice must have less stiffness and lower viscosity in the Kelvin unit (see Fig. 3.1), due to the defects and crystal structure. Both delayed elastic strain and secondary creep strain are enhanced by the defects (this will be discussed later). After a total strain of about 1.5% to 2%, the strain-stress curves begin to converge again, and as mentioned previously, the recoverable strain is less than 10% of the total strain when the stress reaches a plateau, most of the strain is secondary creep strain, i.e., $\epsilon^c \approx \epsilon$; furthermore, the stress σ is almost constant, so, $\dot{\epsilon}^e \approx \dot{\epsilon}^d \approx 0$, this yields

$$\frac{\sigma}{\mu'_f} = \dot{\epsilon}^c_f \approx \dot{\epsilon} \approx \dot{\epsilon}^c_i = \frac{\sigma}{\mu'_i}, \text{ thus} \tag{3.1}$$

$$\mu'_f \approx \mu'_i \tag{3.2}$$

where superscript prime means damaged material properties and the subscripts f and i stand for freshwater ice and multiyear ice, respectively. The equation shows that the two types of ice have similar viscosities. This suggests that in the strain range of 0.1% to 0.5%, as mentioned above, the freshwater ice suffers more damage than that of the multiyear ice due to the much higher stress. Therefore the freshwater ice has been given a great deal of strain softening and viscosity reduction. So the viscosity of ice, which was measured from the constant strain rate test after the plateau, is actually that of damaged ice, not intact ice.

The creep tests provided additional information on the elasticity and viscosity of the ice. Fig. 3.13 shows the strain responses of intact and predamaged ice at a stress of 0.75 MPa (ϵ^e and ϵ'^e are the elastic strains; $\epsilon^d + \epsilon^c$ and $\epsilon'^d + \epsilon'^c$ are delayed elastic strains plus secondary creep strains for intact and predamaged ice, respectively. By focussing on the strain versus time curves close to time = 0, the instantaneous elastic strains can be estimated). The elastic strains and total creep strains at 20 seconds are plotted in Fig. 3.14. The static elastic modulus of intact multiyear ice is estimated as 8000 MPa at -20 °C, and the modulus of predamaged ice is about 6000 MPa at -20 °C . These values are taken from the slopes of the stress-strain curves in Fig. 3.14a, and these elastic responses of the intact multiyear ice show that the small repeated loadings have not added significant damage in the ice. Comparing the creep responses (delayed elastic strain plus secondary creep strain) of the tests of intact to predamaged ice in Fig. 3.14b (see also Fig. 3.13), shows that the presence of cracks and damage significantly influence creep strain. The creep strain of predamaged ice is about 5 to 10 times that of intact ice. As shown in Fig. 3.13, the strain response of the intact ice has mostly recovered, and the permanent viscous strain is close to zero. This suggests that the elastic and delayed elastic components of strain dominate for short load times. The strain response of predamaged ice has a significant percentage of secondary creep, and the delayed elastic strain rate (the slope of the strain versus time curve in Fig. 3.13) is much higher than that of intact ice. This implies that cracking and damage can significantly enhance the creep response of ice (see also Stone et al., 1989; Jordaan et al., 1990a, b).

3.2 Spherical Indention Experiments

3.2.1 Experiment Setup

In April, 1989, a total of eleven tests were preformed on the Hobson's Choice Ice Island. Six of them were spherical indentation tests with speed ranging from 0.3 mm/s to 90 mm/s. The insitu ice temperature was about -14 °C. The tests were carried out in an area of 8 m thick multiyear ice which was attached to the edge of the ice island. A trench 3 m wide, 4 m deep and 100 m long was excavated to conduct the tests. The walls of the trench were roughly smoothed with a chain saw and the test areas were specially machined with a vertically mounted circular saw. The wall opposite the test face was also machined and made parallel to the test face.

The ice indentation system consisted of a hydraulic actuator mounted upon a large mobile skid of beam and strut construction (Fig. 3.15). The actuator was powered by a bank of pressure accumulators and controlled by a servo-control system which provided a constant displacement rate (with exception of no servo-control system being used for the first test, NRC1). The indentation speeds could be assumed constant over the whole test period. Seven 100 mm diameter pressure cells for measuring local pressures were mounted to the front of the indenter. The location of pressure cells is shown in Fig. 3.16. A flat back plate was attached to the rear end of the actuator to support the system. This back plate had a larger contact area than the indenter to force crushing failure on the indentation face only.

3.2.2 Results and Discussion

As discussed in the work of Frederking et al. (1990a, b), both large scale and local crushing under the indenter face typically accompanied the indentation tests. Low speed tests allowed sufficient time for creep deformation and microcracks to extend into the ice, and the total load versus time curves were relatively smooth, while high speed tests appeared to produce localized failure near the indenter and dynamic ice forces on the indenter were recorded. Analysis of crushed layer profiles during spherical indentation tests showed that the layer thickness was irregular. The thickness of the crushed layer was about 20 mm to 50 mm for test No. 7, and the maximum thickness observed was about 320 mm at the center of the contact area during test NRC5. There was a clear boundary between the parent ice and crushed ice. For the low speed tests, the ice under the indenter was partly damaged with short cracks. In the present work, attention is focussed on two of the spherical indentation tests, these are denoted as NRC1 and NRC2, respectively. The load-time results of the two tests are shown in Fig. 3.17a, b. The loading rate for test NRC1 was 0.3 mm/s. The indenter came in contact with the ice at point A and the system stopped at point C. It was observed that a very large piece of ice spalled off during the test, when large cracks extended 6-9 m on either side of the indenter towards the top ice surface. It is believed that the spall occurred at point B, and so the test results after point B have not been used for modelling purposes. A similar situation existed for test NRC2 conducted at 2.5 mm/s, in which two big spalls probably occurred. Here again the portion of the test after point B was neglected.

From the pressure measurements, the maximum pressures were recorded at the center of the indenter and the average pressures were in the range of 5 MPa to 20

MPa. Due to high confining pressure and lower shear stress in the central area, the ice is less damaged (the critical stress required for crack nucleation increases with confining pressure (Kalifa et al., 1989)). Near the edge of the interface, there is less confining pressure and higher shear stress, so the ice has become more damaged and the crushed layer is thicker. Recrystallization due to possible pressure melting has also been reported during indentation tests (Gagnon and Sinha, 1991), which means that friction between the indenter and the ice may be very small.

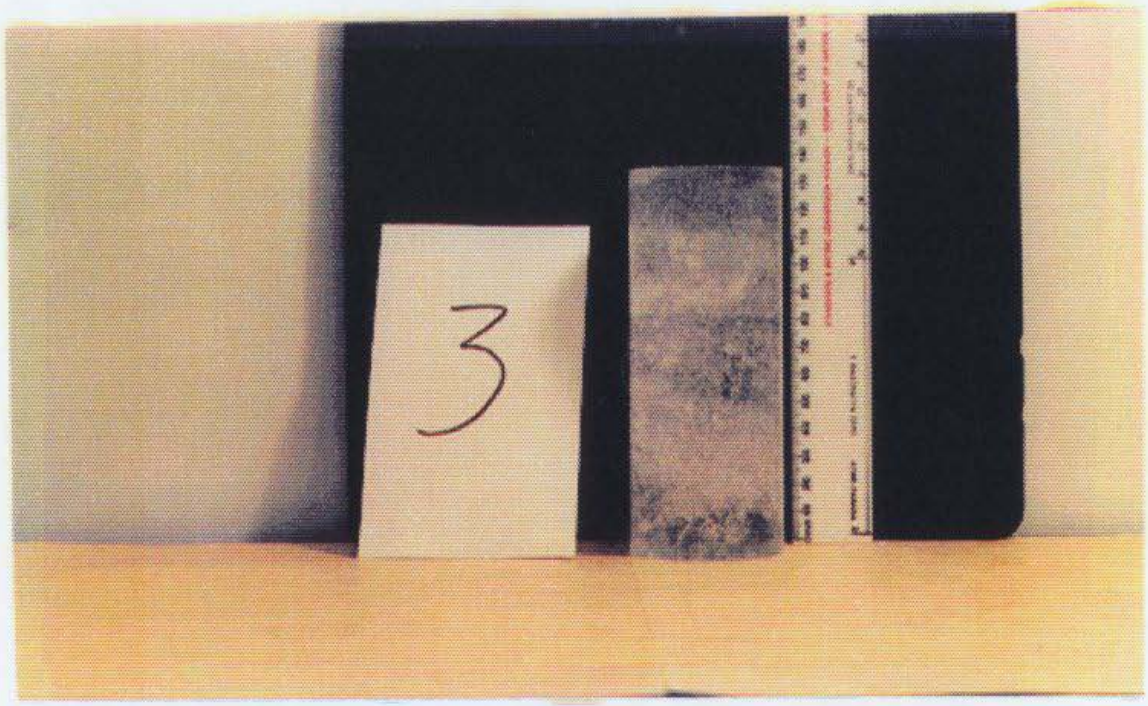

(a)

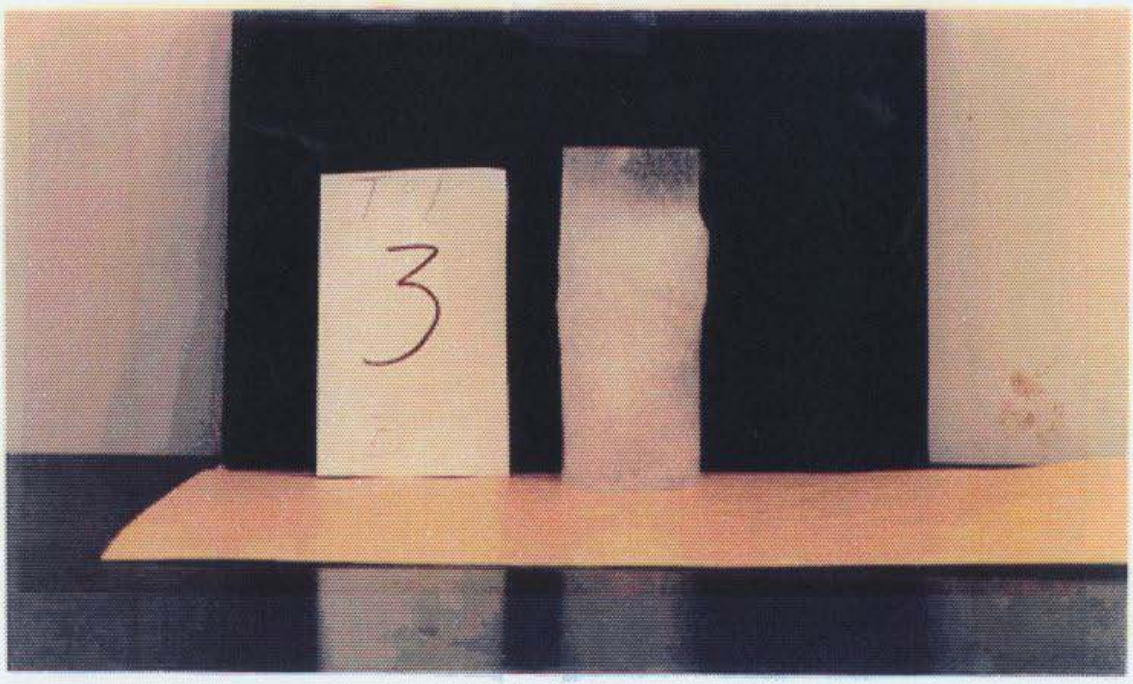

(b)

Figure 3.1: Photograph of ice samples: (a) before test; (b) after test.

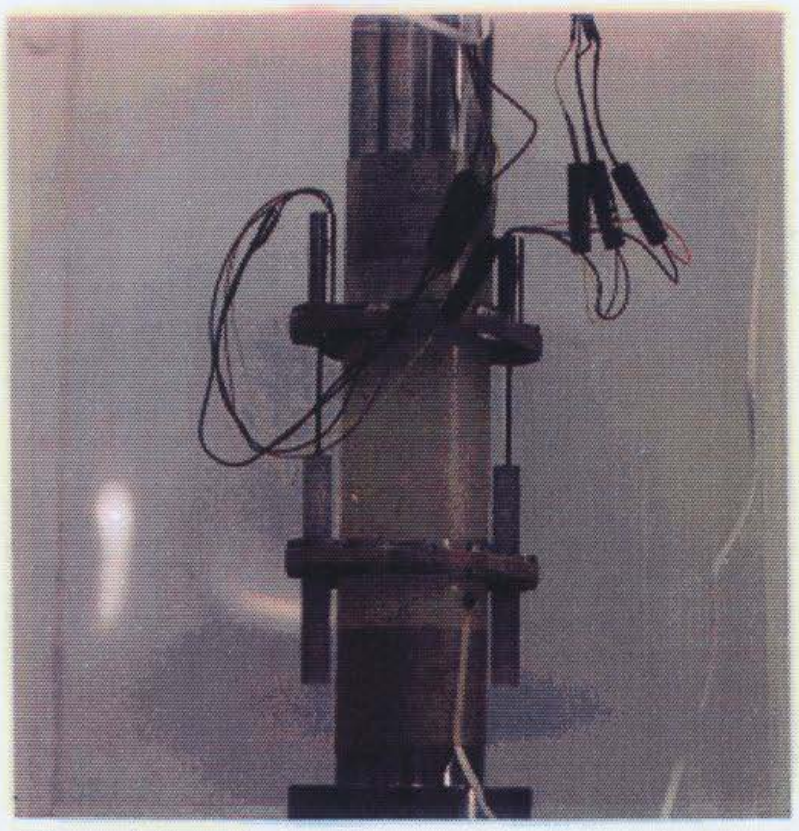

Figure 3.2: Test setup for measuring the axial strain.

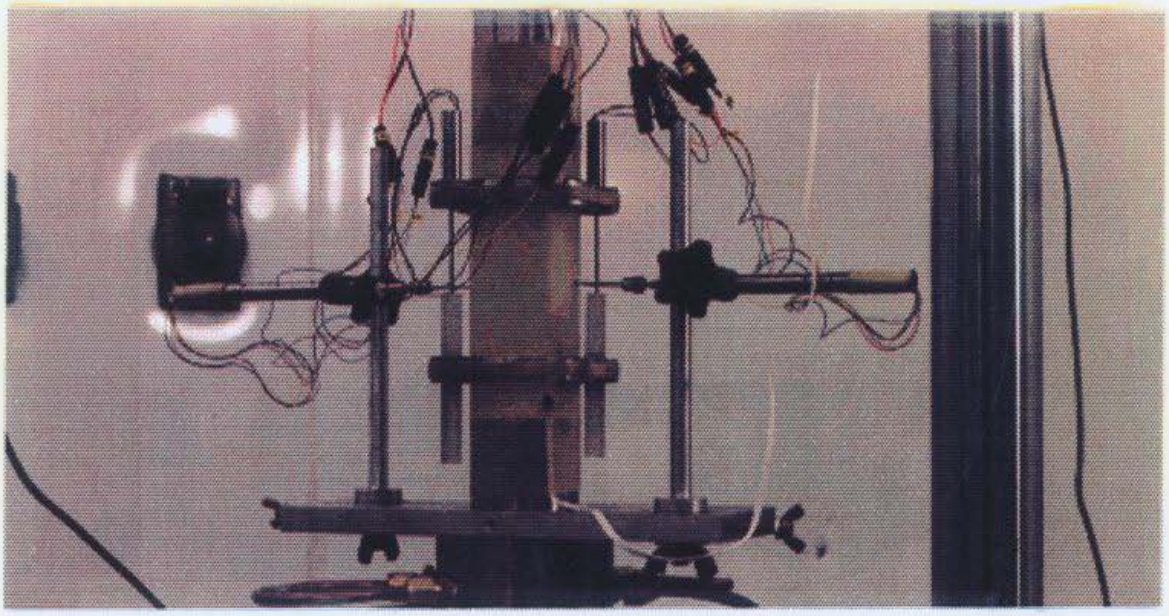

Figure 3.3: Test setup for measuring both axial and lateral strain.

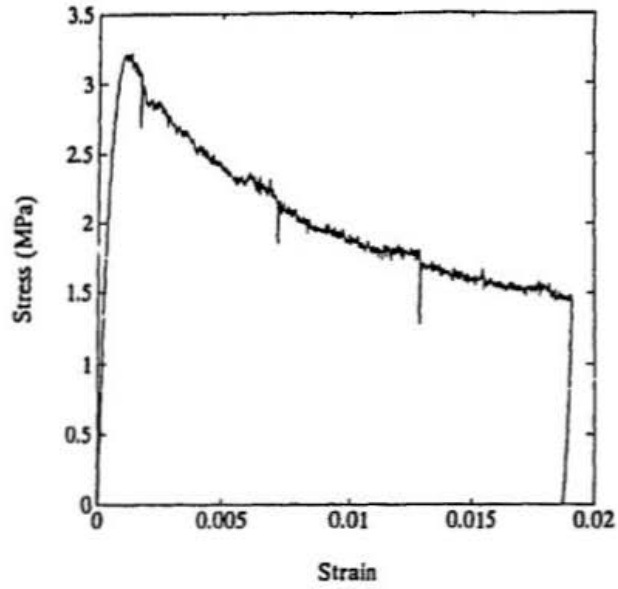

Figure 3.4: Stress-strain curve for uniaxial test No. 1.

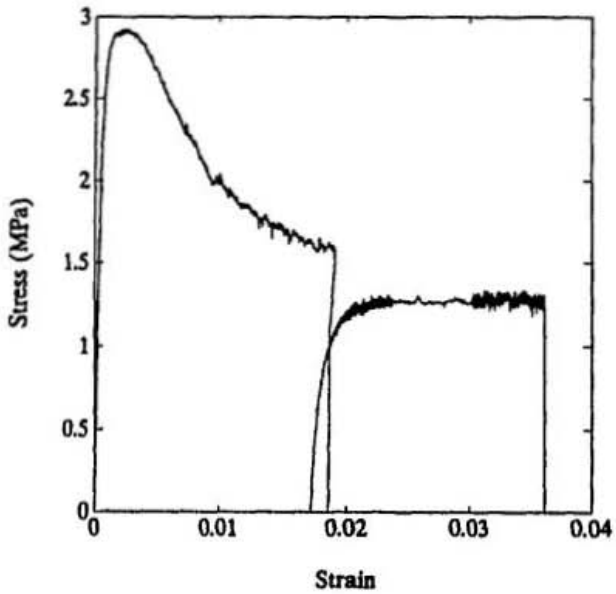

Figure 3.5: Stress-strain curve for uniaxial test No. 2.

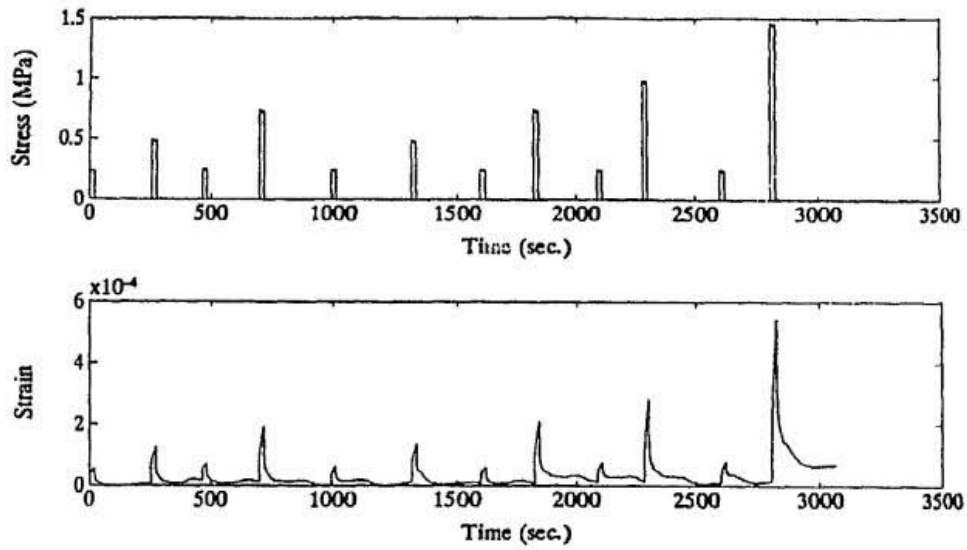

Figure 3.6: Applied stress history and strain response of creep test No. 3.

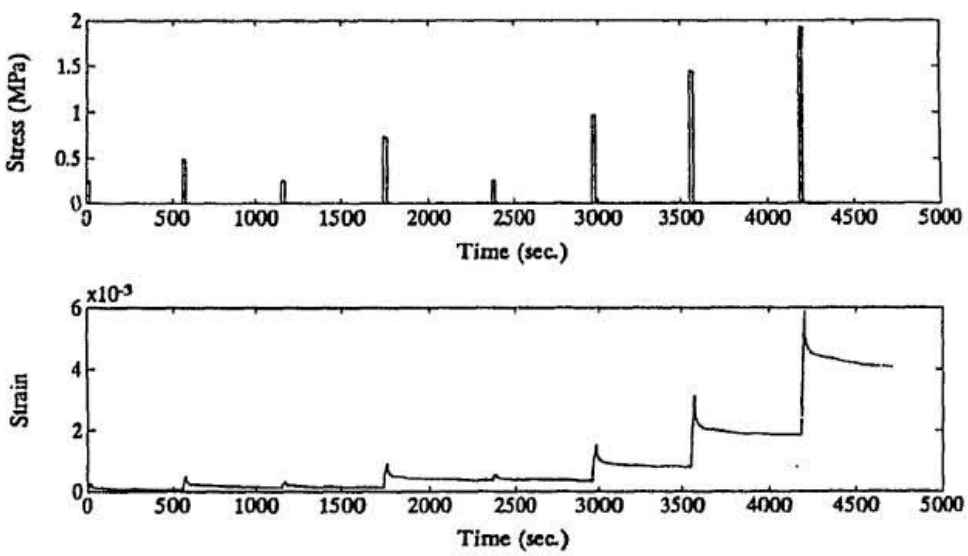

Figure 3.7: Applied stress history and strain response of creep test No. 4.

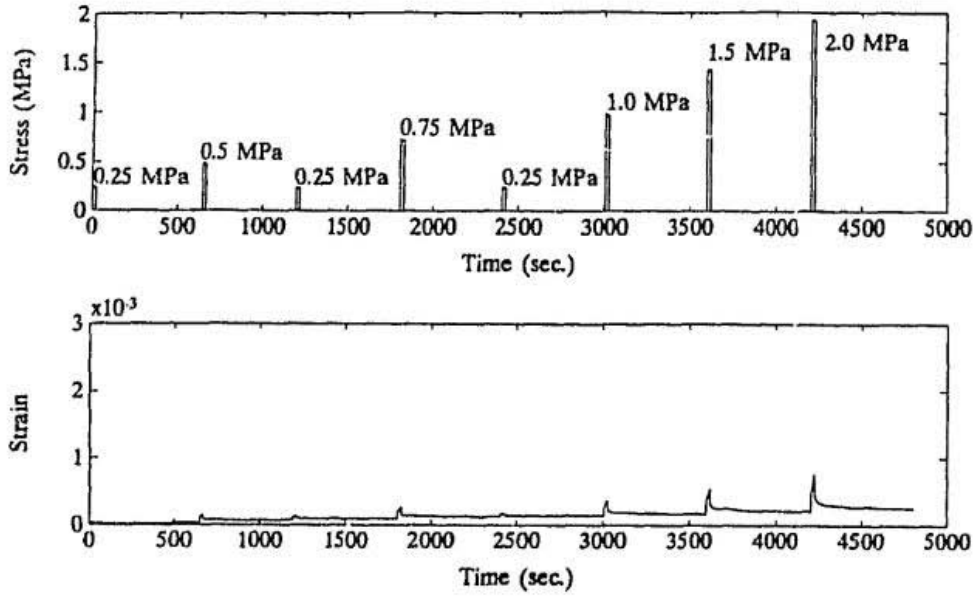

Figure 3.8: Applied stress history and strain response of creep test No. 5.

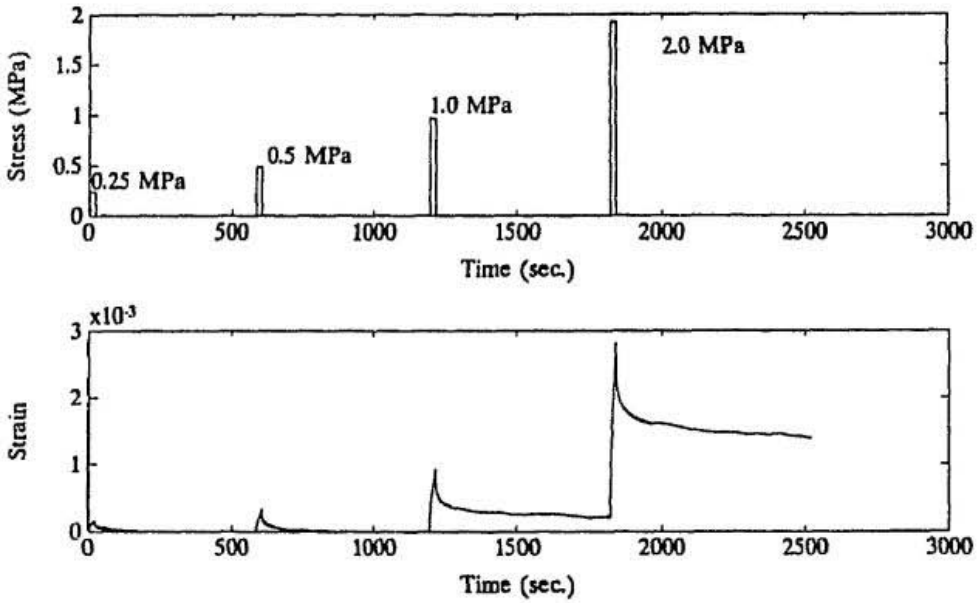

Figure 3.9: Applied stress history and strain response of creep test No. 6.

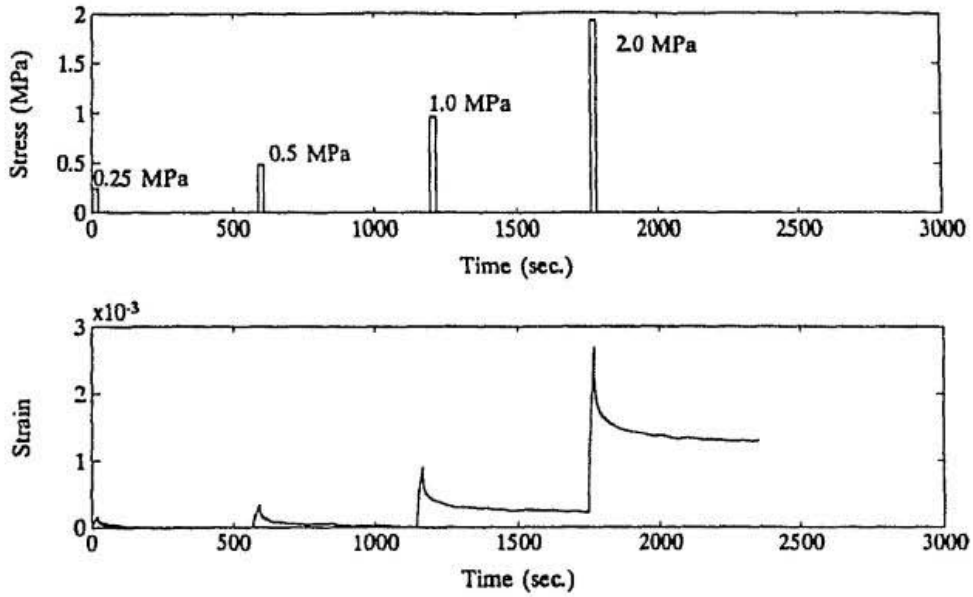

Figure 3.10: Applied stress history and strain response of creep test No. 7.

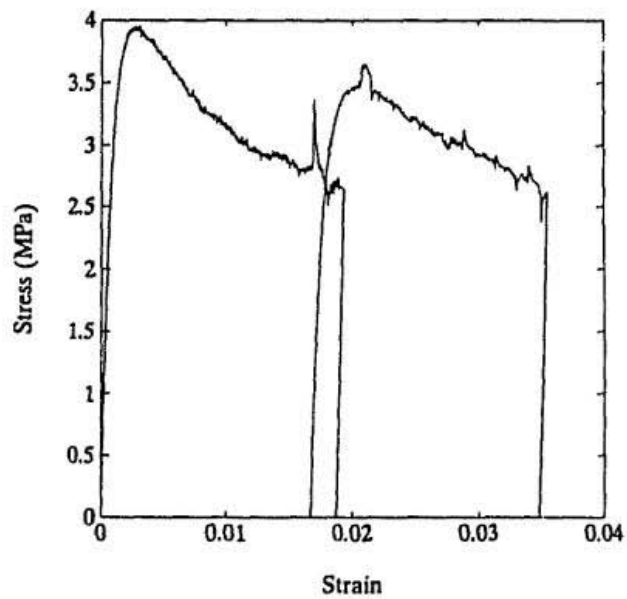

Figure 3.11: Stress-strain curve for uniaxial test No. 8.

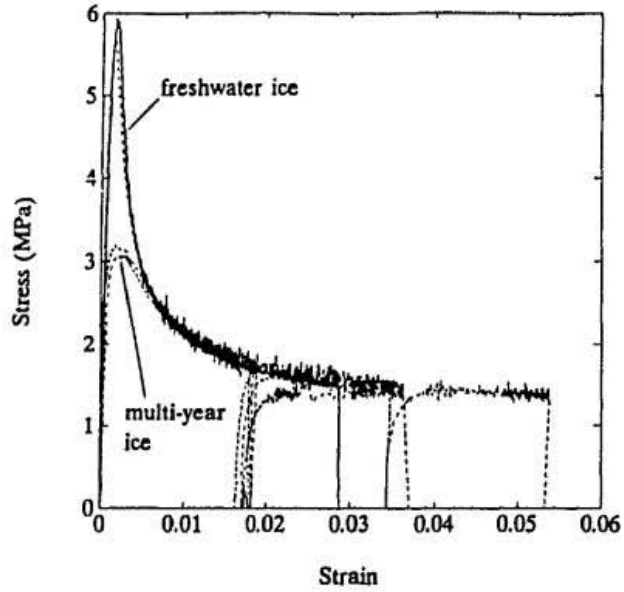

Figure 3.12: Stress-strain curves of constant strain rate tests on both freshwater and multiyear ice at strain rate of $10^{-4}s^{-1}$.

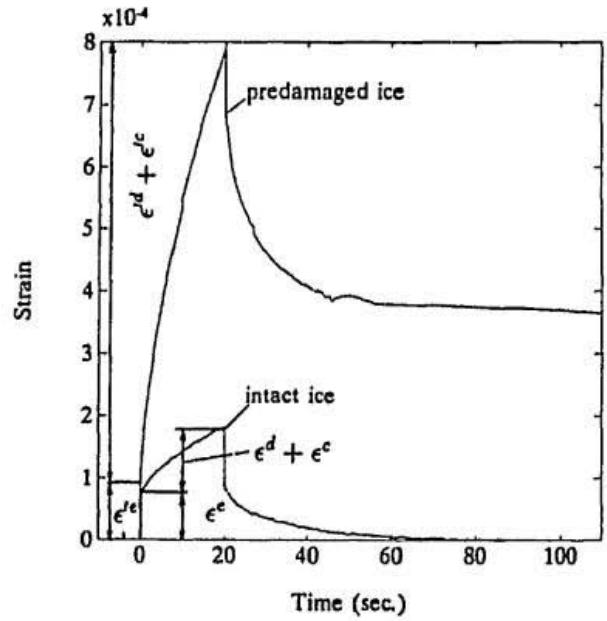

Figure 3.13: Strain responses of intact and predamaged ice for stress at 0.75 MPa.

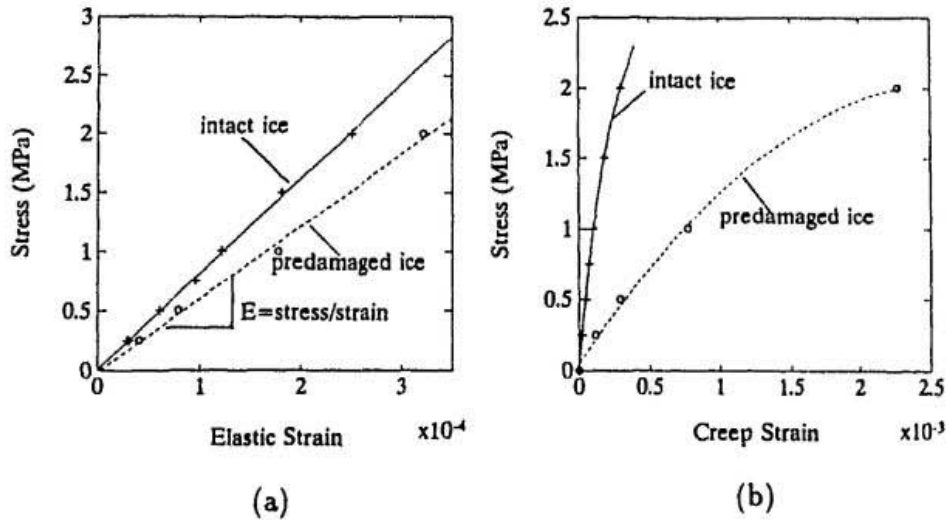

Figure 3.14: Creep tests: (a) stress versus elastic strain for intact and predamaged ice; (b) stress versus total creep strain at 20 seconds after the application of the load for intact and predamaged ice.

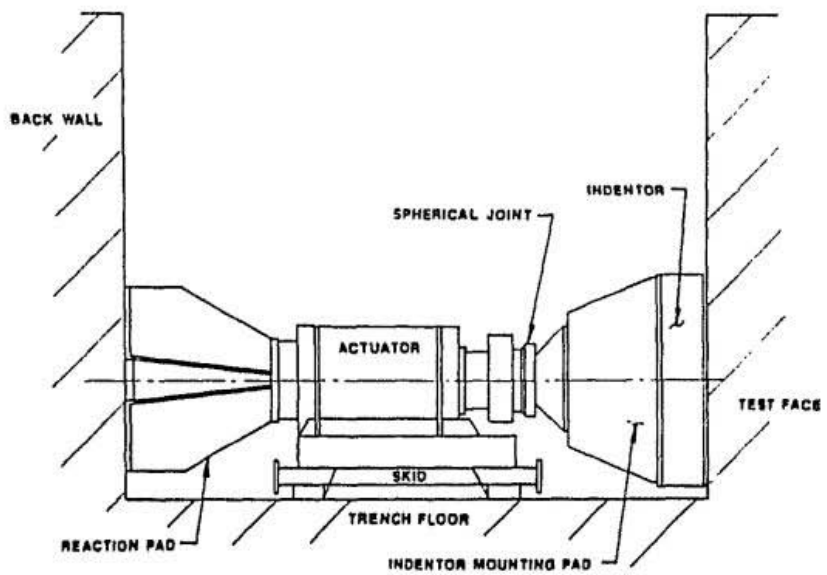

Figure 3.15: Schematic of the actuator indenter system (Frederking et al., 1990a).

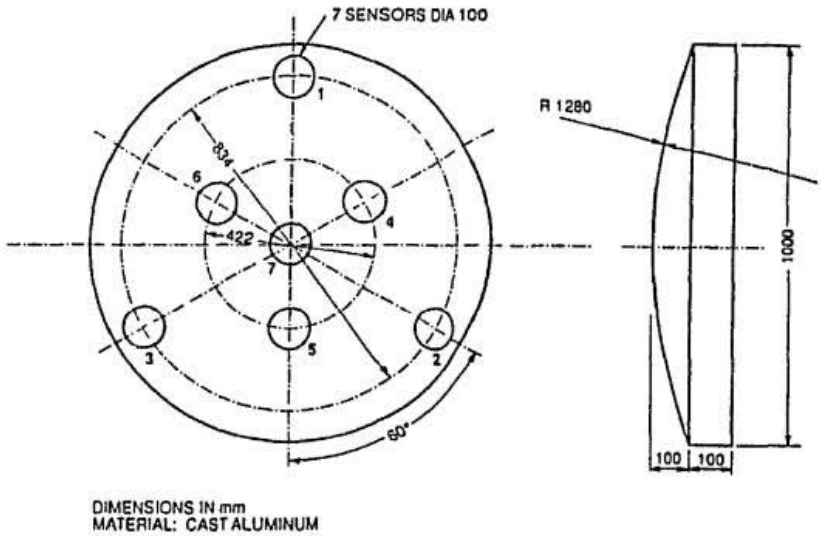

Figure 3.16: Schematic of the spherical indenter and the locations of local pressure cells (Frederking et al., 1990a).

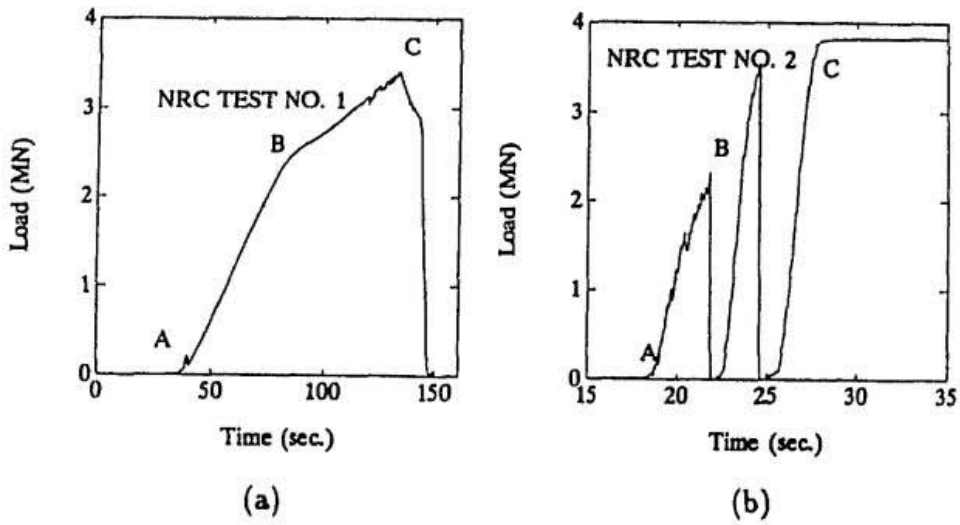

Figure 3.17: The total load versus time records of test: (a) NRC1; (b) NRC2 (Frederking et al., 1990a).

Chapter 4

Constitutive Modelling

4.1 Ice Model

As discussed in the previous chapters, the deformation of ice is a complex process, especially when cracking activity occurs. The properties of ice are strongly influenced by the presence of cracks and damage. The idealized mechanical model, called Burgers' model (see Fig. 2.1), consists of combination of a Maxwell and a Kelvin units, with a nonlinear dashpot in each unit (see also Jordaan and McKenna, 1988b).

Much work has been done to model the primary and secondary creep in ice and other materials. A Kelvin unit with a power-law stress-dependent creep compliance, as proposed by Jordaan and McKenna (1988b, 1989), Jordaan et al., (1990a, b), has been shown to be appropriate for describing the initial primary creep under rapid loading. This also provides an expedient computational solution for the primary creep strain. With this model, at the beginning of each time increment, the program only needs to read the stresses, strains and other model parameters which are stored as state variables from the previous state, instead of requiring access to the whole storage of past history. All of the state variables will be updated at the end of each

increment.

In the case of uniaxial stress, total axial strain is given in terms of three components, i.e.

$$\epsilon_1 = \epsilon_1^e + \epsilon_1^d + \epsilon_1^c \tag{4.1}$$

where the elastic component is given by

$$\epsilon_1^e = \sigma_1 / E, \tag{4.2}$$

where σ_1 is the axial stress and E is the elastic modulus. From the laboratory results of creep tests, Young's modulus of multi-year ice for the static case is approximately 8000 MPa at -20 °C. Since the primary creep properties of ice were estimated based on these results, for consistency, this value is used in the modelling.

The delayed elastic and secondary creep strain rates are defined as

$$\dot{\epsilon}_1^d = \sigma_1 / \mu_{k1}, \text{ and} \tag{4.3}$$

$$\dot{\epsilon}_1^c = \sigma_1 / \mu_{m1} \tag{4.4}$$

where μ_{k1} and μ_{m1} are the viscosity coefficients of the Kelvin unit and Maxwell unit, respectively. Assuming that the strains of the dashpots in both units follow the power-law relation with stress, as given in Eq. (2.5), the delayed elastic strain rate is given as

$$\dot{\epsilon}_1{}^d = \dot{\epsilon}_0^d (\sigma_1^d / \sigma_0)^n \tag{4.5}$$

where $\dot{\epsilon}_0^d$ is a creep reference rate; $\sigma_0 = 1$ MPa, is a constant with unit stress; and σ_1^d is the stress in the dashpot in Kelvin unit, which is calculated by

$$\sigma_1^d = \sigma_1 - E_k \epsilon_1^d \tag{4.6}$$

where E_k is elastic stiffness in the Kelvin unit and following Sinha (1981), it is defined as a function of the grain size

$$E_k = E\frac{d}{c_1 d_1} \tag{4.7}$$

where $c_1 = 9$ is a material constant, $d_1 = 0.001$m and d is the grain size.

The accumulated delayed elastic strain ϵ_1^d is given by

$$\epsilon_1^d = \int_0^t \dot{\epsilon}_1^d \, dt. \tag{4.8}$$

Comparing Eq. (4.3) with Eq. (4.5), it is found that

$$\mu_{k1} = (\sigma_1/\dot{\epsilon}_0^d)(\sigma_0/\sigma_1^d)^n. \tag{4.9}$$

Similarly, the secondary creep strain rate is also assumed to follow the power-law with stress, i.e.

$$\dot{\epsilon_1}^c = \dot{\epsilon}_0^c(\sigma_1/\sigma_0)^n \tag{4.10}$$

where $\dot{\epsilon}_0^c$ is a creep parameter. So the viscosity coefficient of Maxwell unit is defined as

$$\mu_{m1} = (\sigma_1/\dot{\epsilon}_0^c)(\sigma_0/\sigma_1)^n. \tag{4.11}$$

From the creep tests on intact ice (see discussions in Chapter 3), it is found that, under rapid loading, delayed elastic strain rate is much higher than that of secondary creep strain. In light of Eq. (4.6), the stress in the dashpot of Kelvin unit σ_1^d is smaller than the overall stress σ_1. In order to fit the measured data, the

viscosity of the Kelvin unit must be much lower than that of the main dashpot. Hence, the viscosity parameter $\dot{\epsilon}_0^d$ is assumed simply to be proportional to that of main dashpot $\dot{\epsilon}_0^c$, i.e.

$$\dot{\epsilon}_0^d = c' \dot{\epsilon}_0^c \tag{4.12}$$

where c' is a material constant.

In the case of multi-axial stress state, the deformation of ice is then written in the form of

$$\epsilon_{ij} = \epsilon_{ij}^e + \epsilon_{ij}^d + \epsilon_{ij}^c \tag{4.13}$$

as given in Eq. (2.16). If the elastic properties of ice are assumed to be isotropic, the stress-strain relationship can be expressed by

$$\sigma_{ij} = (K - \frac{2}{3}G)\epsilon_{kk}^e \delta_{ij} + 2G\epsilon_{ij}^e \tag{4.14}$$

where K is bulk modulus; G is shear modulus and δ_{ij} is the delta function.

Both delayed elastic strain and secondary creep strain can be expressed in terms of a strain deviator component e_{ij} and a volumetric strain component ϵ_v, i.e.

$$\epsilon_{ij}^d = e_{ij}^d + \epsilon_v^d, \text{ and} \tag{4.15}$$

$$\epsilon_{ij}^c = e_{ij}^c + \epsilon_v^c. \tag{4.16}$$

Note that the volumetric strains here are not the results of elastic deformation (compaction or dilatation); if the ice creep behaviour is assumed to be incompressible, they are the nonlinear dilatation probably due to the cracking and some other mechanisms which will be discussed in the next section. As addressed in Chapter

3, elastic strain plus delayed elastic strain is about or less than 10% of the total strain during constant strain-rate tests. Since there is no clear evidence showing that a portion of the nonlinear dilatation is directly related to the delayed elastic strain, the volumetric strain component ϵ_v^d is assumed to be negligible and the total nonlinear dilatation ϵ_v is equal to ϵ_v^c.

Based on the discussions in the case of uniaxial loading, the deviatoric strain rates of delayed elastic and secondary creep components are assumed to be proportional to the deviatoric stresses and are defined in the forms similar to Eq. (4.3) and Eq. (4.4)

$$\dot{e}_{ij}^d = \frac{3}{2} s_{ij}/\mu_k, \text{ and} \tag{4.17}$$

$$\dot{e}_{ij}^c = \frac{3}{2} s_{ij}/\mu_m \tag{4.18}$$

where $s_{ij} = \sigma_{ij} - \frac{1}{3}\sigma_{ii}$ is the overall stress deviator. These definitions assume that ice creep behaviour is isotropic, and the viscosity coefficient of shear deformation follows the same law as that in the principal directions.

The viscosity coefficients, μ_{k1} and μ_{m1} defined in Eq. (4.3) and Eq. (4.4) are functions of axial stress. In the case of multi-axial loading, the coefficients, μ_k and μ_m are defined as functions of von Mises stress in the similar ways, by substituting the axial stress component with von Mises stress, i.e.

$$\mu_k = (s/\dot{\epsilon}_0^d)(\sigma_0/s^d)^n, \text{ and} \tag{4.19}$$

$$\mu_m = (s/\dot{\epsilon}_0^c)(\sigma_0/s)^n. \tag{4.20}$$

The definition of von Mises stress is given as

$$s = (\frac{3}{2}s_{ij}s_{ij})^{1/2}. \tag{4.21}$$

If incompressible behaviour is assumed for creep strain and $\epsilon_v^d = 0$, the internal stress s^d (the von Mises stress in the dashpot in the Kelvin unit), is calculated by

$$s^d = s - E_k e^d \tag{4.22}$$

where e^d is the equivalent (or effective) delayed elastic strain which is calculated by

$$\begin{aligned} e^d &= \int_0^t \dot{e}^d \, dt \\ &= \int_0^t \dot{\epsilon}_0^d (s^d/\sigma_0)^n \, dt. \end{aligned} \tag{4.23}$$

The definition of equivalent strain is given by

$$e = (\frac{2}{3}e_{ij}e_{ij})^{1/2}. \tag{4.24}$$

Reference can be made to Appendix A for more details on the definition of equivalent strain and its relationship with von Mises stress.

Substituting Eq. (4.19), Eq. (4.22) into Eq. (4.17), and Eq. (4.20) into Eq. (4.18), it is found that

$$\begin{aligned} \dot{e}_{ij}^d &= \frac{3}{2}\dot{\epsilon}_0^d \left(\frac{s^d}{\sigma_0}\right)^n \frac{s_{ij}}{s} \\ &= \frac{3}{2}\dot{\epsilon}_0^d \left(\frac{s - E_k e^d}{\sigma_0}\right)^n \frac{s_{ij}}{s}, \quad \text{and} \end{aligned} \tag{4.25}$$

$$\dot{e}_{ij}^c = \frac{3}{2}\dot{\epsilon}_0^c \left(\frac{s}{\sigma_0}\right)^n \frac{s_{ij}}{s}. \tag{4.26}$$

In the case of uniaxial loading, deviatoric stresses $s_{11} = \frac{2}{3}\sigma_1$, $s_{22} = s_{33} = -\sigma_1/3$ and $s_{ij} = 0, (i \neq j)$, so von Mises stress $s = \sigma_1$; therefore, $s^d = \sigma_1^d$; similarly,

the deviatoric delayed elastic strains $e^d_{11} = \epsilon^d_{11} - \epsilon^d_v = \epsilon^d_{11}$ (assuming $\epsilon^d_v = 0$), $e^d_{22} = e^d_{33} = \epsilon^d_{22} = -\epsilon^d_{11}/2$, thus $e^d = \epsilon^d_{11} = \epsilon^d_1$. Therefore, the above two equations become

$$\dot{e}^d_{11} = \dot{\epsilon}^d_0 \left(\frac{\sigma_1 - E_k \epsilon^d_1}{\sigma_0} \right)^n \text{ and} \tag{4.27}$$

$$\dot{e}^c_{11} = \dot{\epsilon}^c_0 (\sigma_1/\sigma_0)^n. \tag{4.28}$$

These two equations are equivalent to Eq. (4.5) and Eq. (4.10). So it is consistent and convenient to assume that the viscosity coefficients, μ_k and μ_m are related to the von Mises stress and equivalent strain, since the constants of ice properties are calibrated from the uniaxial test results.

When rapid loading is applied, the dashpot in the Kelvin unit carries most of the load at the beginning for a very short time, i.e. $s^d \approx s$. Since $s^d \propto \dot{e}^d$, and the stress in the spring is proportional to the strain e^d, the influence of the elastic effect on $\dot{\epsilon}^d_{ij}$ is reduced, and the delayed elastic strain can then be modelled as a viscous element in the same way as $\dot{\epsilon}^c_{ij}$, but with significantly softer viscous behaviour.

4.2 Dilatation of Ice

Only in recent years, more attention has been paid to the dilatation of ice on loading, especially when cracking and damage is induced. As addressed in the discussion of the previous chapter, the density of ice in the crushed layer adjacent to the indenter (Frederking et al., 1990a, b) was less than that of parent ice, indicating the presence of dilatation due to the cracking and pulverizing of the ice during the interaction process. Dilatation was also measured in small scale

compressive experiments at constant strain rates by Wang (1981), Dorris (1989) and at constant stress by Sinha (1989).

Sinha (1989) observed dilatation due to crack formation for S-2 ice subject to constant uniaxial compressive loads ranging from 1.2 MPa to 3 MPa. Some triaxial compressive tests on multi-year sea ice were conducted by Dorris (1989) at -5°C for constant strain rates of $10^{-3}s^{-1}$ and $10^{-2}s^{-1}$. The constant confining pressures were 2.62 MPa and 10 MPa. The structure of the ice samples was basically granular or mixed granular and columnar ice with an average salinity of 0.26 $\pm$ 0.19 $^{o}/_{oo}$ and the average density of 0.902 $\pm$ 0.14 g/cm^3. The tests were loaded to a total axial strain of 10%, which is a relatively large strain. Two techniques were used to obtain volumetric strain; measuring the diametral expansion of the sample in two orthogonal directions at its midpoint, or measuring the fluid volume change within the confining cell. The stress-strain curves of four tests were presented in Dorris (1989) and shown in Fig. 4.1. The corresponding volumetric strains measured from changes in fluid volume and in diameter are shown in Fig. 4.2, which are found to increase with increased loading rate and decreased confining pressure, and have about the same order as the axial deformation. In the paper, compaction was defined as being positive while dilatation was negative. Digitizing the volumetric strain curves and stress-strain curves at the axial strain of 2%, 3% and 4%, it is found that the ratio of volumetric strain to axial strain are almost constant when the axial strain is larger than 2%. So ignoring the elastic strains, volumetric strain rate is modelled as a function of the confining stress and axial stress. The ratio of volumetric strain rate to equivalent strain rate (nonlinear part) was plotted as a function of the ratio of confining stress to axial stress for axial strains of 4% (see

Fig. 4.3). An exponential function was proposed to fit the data (McKenna et al., 1990)

$$\dot{\epsilon}_v/\dot{e} = 0.25 \exp(1.5\sigma_v/s); \quad \sigma_v \leq 0 \tag{4.29}$$

where σ_v is the volumetric stress. Note that the volumetric strain rate is assumed to be positive for dilatation. This equation is only valid for compression since the test data were obtained from compressive tests with relatively high confining pressure. Notice that the measured volumetric strain is not only due to cracking. The high confining pressure may close some or most of the cracks. According to Horii and Nemat-Nasser (1983), when the confining stress, or the normal stress of the crack surface, is larger than the shear stress transmitted across the crack surface, the crack wili be closed. In the case of triaxial loading, the maximum shear stress is a half of the axial stress $\sigma_{11}-\sigma_{33}$, and the normal stress is equal to $(\sigma_{11}+\sigma_{33})/2$, when the crack surface is at 45° to the axial direction. For the tests shown in Fig. 4.1, the normal stress was always larger than the shear stress, hence the cracks should be closed. In this case cracks may not dominate the dilatation of ice. Dilatation could be the result of the combined influence of grain boundary sliding and creep around the crack tips (Jordaan et al., 1990b). There is not much information about the dilatation of ice in tension, and in the present work most states of stress are compressive, so when σ_v is positive (in tension), volumetric strain rate is assumed to be zero. Conversely, the influence of randomly oriented open microcracks on the elastic properties of a material has been discussed by Budiansky and O'Connell (1976). A general method based on a self-consistent approach was developed to estimate the overall moduli which are the functions of the crack density. Hence the

volumetric strain in tension due to cracking can be calculated, this will be discussed in detail later.

Finally, the strain rate tensor is expressed by

$$\dot{\epsilon}_{ij} = \dot{\epsilon}^e_{ij} + \dot{\epsilon}^d_{ij} + \dot{\epsilon}^c_{ij} + \delta_{ij}\dot{\epsilon}_v. \tag{4.30}$$

where $\dot{\epsilon}^e_{ij}, \dot{\epsilon}^d_{ij}$ and $\dot{\epsilon}^c_{ij}$ are elastic, delayed elastic and secondary creep strain tensor, respectively; $\dot{\epsilon}_v$ is the volumetric strain (nonlinear part).

4.3 Damage Evolution Law

Damage mechanics has only recently been applied to ice. Damage evolution depends on stress, strain, loading rate, as well as cracks and damage state. Budiansky and O'Connell (1976) discussed the reduction of elastic moduli due to the presence of microcracks of a given shape for a three dimensional case. Their solution calculates the change of elastic properties from the strain energy loss during the nucleation of individual cracks in an elastic brittle body. Their results include interaction between cracks but do not account for traction across crack surfaces; all cracks remain open. Assuming an isotropic array of similarly shaped flat circular cracks, the isotropic damage parameter is simply related to the crack density by

$$D_N = a^3 N, \tag{4.31}$$

where a is the radius of crack surface and N is the crack density. According to Cole (1986), the average crack size is about 0.65 times the average ice grain size, but for simplicity, the crack size is assumed to equal to the grain size and by altering the constant, then

$$D_N = N/(8N_g);\ N_g = d^{-3} \tag{4.32}$$

where d is the average grain size. For cracks of certain shapes, the relation between crack density and the elastic moduli, and Poisson's ratio are given detail in Budiansky and O'Connell (1976). For flat circular cracks, which is assumed to be the case in ice, the functions are given as

$$K'/K = 1 - [16(1 - \nu'^2)]/[9(1 - 2\nu')]\, D_N \tag{4.33}$$

$$G'/G = 1 - [32(1 - \nu')(5 - \nu')]/[45(2 - \nu')]\, D_N \tag{4.34}$$

and

$$E'/E = 1 - [16(1 - \nu'^2)(10 - 3\nu')]/[45(2 - \nu')]\, D_N \tag{4.35}$$

with

$$D_N = [45(\nu - \nu')(2 - \nu')]/[16(1 - \nu'^2)(10\nu - \nu'(1 + 3\nu))], \tag{4.36}$$

where the prime denotes that the property includes the effect of cracks. Some results were given in the paper and are plotted in Fig. 4.4, which shows that the Poisson's ratio, shear and Young's moduli decrease almost linearly with damage; the two moduli are not strongly dependent on ν, so the last three equations can be simplified as

$$\nu'/\nu \approx 1 - (16/9)D_N;\ D_N < 9/16. \tag{4.37}$$

$$G'/G \approx 1 - (16/9)D_N;\ D_N < 9/16. \tag{4.38}$$

$$E'/E \approx 1 - (16/9)D_N;\ D_N < 9/16. \tag{4.39}$$

The bulk modulus is also a linear function of damage when ν is very small. That is

$$K'/K \approx 1 - (16/9)D_N;\ D_N < 9/16. \tag{4.40}$$

When ν increases, the bulk modulus will initially decrease rapidly and the rate of decrease slows with increasing D_N. Recall that these solutions are only valid for randomly oriented open cracks where there are no traction or friction on the crack surfaces.

Under compression, the effect of traction across cracks can not be ignored and the above approach needs to be modified. It is comprehensible that the influence of cracks on the elastic properties will be reduced in compression due to the crack closure and difficulty in crack nucleation. The closed cracks can still transform traction and shear stress, so in compression, the existence of cracks will not reduce the strength of the solid body as much as in tension. Horii and Nemat-Nasser (1983) developed a general solution for the case of two dimensional, plane strain, compressive state of stress. Some results were presented in the paper and shown in Fig. 4.5. From their calculation, the reduction of all elastic properties is smaller in compression (cracks closure) than in tension (cracks open). Their solutions must be solved numerically. So in present work, for an approximation, simple relations were proposed as

$$G'/G = 1 - \omega D_N, \text{ and} \tag{4.41}$$

$$K'/K = 1 - \omega D_N \tag{4.42}$$

where $\omega = 16/9$ in tension, the above expressions approximate those given by Budiansky and O'Connell (1976). For compressive stress states, $\omega = 1$. This is an

approximation of the work of Horii and Nemat-Nasser (1983). As discussed in the previous chapters, with increasing damage, the elastic strain becomes small relative to the total strain. For a high degree of damage, the total strain is dominated by creep strain and the elastic strain is not significant. The specification of G' and K' is therefore not critical. Additionally, for small degrees of damage, Eq. (4.41) and Eq. (4.42) were found to produce good approximations of the moduli.

4.4 Crack Nucleation

Extensive experimental work has been performed to investigate crack nucleation and crack density development in ice (Gold, 1972, Cole, 1986, Hallam et al., 1987, Sinha, 1984, 1989b). Much of this work has been conducted with small scale compressive tests in laboratory settings. Unfortunately this work does not exactly represent large scale ice-structure interaction, but no additional information is available at this time. Theoretical modelling of crack development has been carried out recently by Jordaan and McKenna (1989), Jordaan et al., (1990a, b), McKenna et al., (1989, 1990) and Sinha (1989). Following McKenna et al. (1990), the rate expression of crack formation;

$$\dot{N} = \dot{N}_c \left(\frac{s - \sigma_c}{\sigma_0} \right)^m \tag{4.43}$$

is used in the present model.

As discussed in Schulson (1987, 1989) and Hallam (1986), the critical stress for crack nucleation is a function of grain size

$$\sigma_c = a_1 + a_2 d^{-1/2},$$

where a_1 and a_2 are constants calculated from critical tensile strain $\epsilon_c = 5.7 \times 10^{-5} + 3.33 \times 10^{-6}\, d^{-1/2}$, i.e., $\sigma_{ct} = E\,\epsilon_c$ for tension and $\sigma_{cc} = E\,\epsilon_c/\nu$ for compression. From Kalifa et al. (1989) the critical stress is also dependent on the confining stress

$$\sigma_c = a_3 + a_4\,\sigma_3, \quad (\sigma_3 \text{ is the confining stress })$$

It seems reasonable to assume that the critical stress σ_c in compression is dependent on grain size and confining stress, and can be expressed as

$$\sigma_c = a_1 + a_2\, d^{-1/2} + a_3\sigma_3, \tag{4.44}$$

since the elastic modulus of multi-year ice E = 8000 MPa and Poisson's ratio ν = 0.3, a_1 is 1.52 MPa and a_2 is 0.0888 MPa m^{-3}. In the case of triaxial compression, von Mises stress is

$$s = \sigma_1 - \sigma_3$$

where σ_1 is the stress in the direction of loading axis and σ_3 is the confining stress. The mean stress is

$$\sigma_v = (1/3)(\sigma_1 + 2\sigma_3), \text{ so that}$$

$$\sigma_v = (1/3)(s + \sigma_3 + 2\sigma_3), \text{ and}$$

$$\sigma_3 = \sigma_v - s/3, \quad (\sigma_3 \text{ and } \sigma_v \leq 0)$$

In Kalifa (1990), parameter a_3 is given as -0.4, thus

$$\sigma_c = 1.52 + 0.0888\, d^{-1/2} - 0.4(\sigma_v - s/3); \quad \sigma_v \leq 0. \tag{4.45}$$

It is also found from the uniaxial tests and the theoretical modelling practice that the critical stress should also be influenced by the existing cracks and damage. Therefore it is proposed that

$$\sigma_c' = \sigma_c(1 - \omega_c D_N) \tag{4.46}$$

where ω_c is a constant and σ_c is given in Eq. (4.45).

There is not much information about the influence of confining pressure on crack nucleation in tension, and this case is rare, so following Schulson and Cannon (1984), it is proposed that in tension the critical stress is

$$\sigma_c' = (0.456 + 0.0266\, d^{-1/2})(1 - \omega_c D_N); \quad \sigma_v > 0. \tag{4.47}$$

4.5 Creep Enhancement

The effect of cracks on the steady-state creep rate for the two dimensional case was examined by Weertman (1969) using dislocation theory. Approximate solutions were given for materials obeying the power law creep equation. His result for low crack density was used by Sinha (1988) as given in Eq. (2.33) where the creep strain is enhanced by a factor of $2\pi N a^2 n^{1/2}$. For high crack density ($a^2 N \gg 1$), Weertman noted that the creep rates must be on the order of

$$\dot{\epsilon}^c \sim A\sigma^n (a^2 N)^{n+1} \tag{4.48}$$

where a is half of the crack size and N is the crack density, which means that the creep enhancement is on the order of $(a^2 N)^{n+1}$. Jordaan and McKenna (1989) proposed a solution for the three dimensional case, as given in Eq. (2.37). The exponential form models the creep enhancement on inelastic strain, which was

redefined as $\exp(\beta D_N)$ in McKenna et al. (1990). This term is actually equal to the series $\sum_{k=0}^{\infty} b_k D_N^k$, where b_k are constants, so it will approximate the linear solution for small D_N ($D_N = Na^3$) and covers all orders of n for $(Na^3)^{n+1}$ at large D_N. Therefore, it is a more general form of the creep enhancement factor. So the creep strain rates of damaged ice are described as

$$\dot{e}_{ij}^{d'} = \dot{e}_{ij}^{d} \exp(\beta_d D_N), \text{ and} \tag{4.49}$$

$$\dot{e}_{ij}^{c'} = \dot{e}_{ij}^{c} \exp(\beta_c D_N) \tag{4.50}$$

where the primes refer to the parameters for the cracked ice; β_d, β_c are constant enhancement parameters, and $\dot{e}_{ij}^{d}$ and $\dot{e}_{ij}^{c}$ are given in Eq. (4.25) and Eq. (4.26), respectively.

4.6 Finite Element Implementation and Model Verification

The numerical solution of damage equations is performed using an explicit incremental scheme. For the stress tensor given by

$$\sigma_{ij} = K_{ijkl}\epsilon_{kl}^{e}, \tag{4.51}$$

where

$$K_{ijkl} = (K - \frac{3}{2}G)\delta_{ij}\delta_{kl} + G(\delta_{ik}\delta_{jl} + \delta_{il}\delta_{jk}), \tag{4.52}$$

the increment of stress tensor is calculated by

$$\delta\sigma_{ij} = K_{ijkl}\delta\epsilon_{kl}^{e} + \delta K_{ijkl}\epsilon_{kl}^{e} \tag{4.53}$$

where the stiffness matrix is given by

$$K_{ijkl} = \begin{Bmatrix} K+4G/3 & K-2G/3 & K-2G/3 & 0 & 0 & 0 \\ & K+4G/3 & K-2G/3 & 0 & 0 & 0 \\ & & K+4G/3 & 0 & 0 & 0 \\ & & & 2G & 0 & 0 \\ & SYMM. & & & 2G & 0 \\ & & & & & 2G \end{Bmatrix}. \qquad (4.54)$$

The incremental change in the elastic stiffness tensor δK_{ijkl} is obtained by first calculating the increment in damage with Eq. (4.31) and Eq. (4.43):

$$\begin{aligned} \delta D_N &= a^3 \delta N \\ &= a^3 \dot{N}_c \left(\frac{s - \sigma_c}{\sigma_0} \right)^m \delta t. \end{aligned} \qquad (4.55)$$

where δt is the time increment specified by the user. Summing this to the accumulated total damage and calculating the difference between the elastic parameters for the current and previous states with Eq. (4.41) and Eq. (4.42), i.e.

$$K' = K[1 - \omega(D_N + \delta D_N)]$$

$$\begin{aligned} \delta K &= K' - K(1 - \omega D_N) \\ &= -K \omega \delta D_N, \end{aligned} \qquad (4.56)$$

similarly,

$$\delta G = -G \omega \delta D_N, \qquad (4.57)$$

thus

$$\delta K_{ijkl} = \begin{Bmatrix} \delta K + 4\delta G/3 & \delta K - 2\delta G/3 & \delta K - 2\delta G/3 & 0 & 0 & 0 \\ & \delta K + 4\delta G/3 & \delta K - 2\delta G/3 & 0 & 0 & 0 \\ & & \delta K + 4\delta G/3 & 0 & 0 & 0 \\ & & & 2\delta G & 0 & 0 \\ & SYMM. & & & 2\delta G & 0 \\ & & & & & 2\delta G \end{Bmatrix}. \qquad (4.58)$$

The increment of elastic strain components $\delta\epsilon^e_{ij}$ is calculated by

$$\delta\epsilon^e_{ij} = \delta\epsilon_{ij} - \delta e^{d'}_{ij} - \delta e^{c'}_{ij} - \delta\epsilon_v \delta_{ij} \tag{4.59}$$

where the total strain increment $\delta\epsilon_{ij}$ is defined in the boundary condition, i.e., the indentation speed or strain rate $\dot{\epsilon}$ and the time increment δt; δ_{ij} is the delta function. The delayed elastic strain increment of undamaged ice, δe^d_{ij}, is calculated from Eq. (4.25) as

$$\delta e^d_{ij} = \frac{3}{2}\dot{\epsilon}^d_0 \left(\frac{s - E_k e^d}{\sigma_0}\right)^n \frac{s_{ij}}{s}\,\delta t. \tag{4.60}$$

Substituting this equation into Eq. (4.49), the delayed elastic strain increment of damaged ice is found to be

$$\delta e^{d'}_{ij} = \dot{\epsilon}^d_0 \left(\frac{s - 2G_k\, e^d}{\sigma_0}\right)^n \exp(\beta_d D_N)\,\frac{s_{ij}}{s}\,\delta t. \tag{4.61}$$

Similarly, the secondary creep strain increment $\delta e^{c'}_{ij}$ can be obtained from Eq. (4.26) and Eq. (4.50), i.e.

$$\delta e^{c'}_{ij} = \dot{\epsilon}^c_0 \left(\frac{s}{\sigma_0}\right)^n \exp(\beta_c D_N)\,\frac{s_{ij}}{s}\,\delta t. \tag{4.62}$$

The volumetric strain increment $\delta\epsilon_v$ is given by Eq. (4.29),

$$\delta\epsilon_v = 0.25\,\exp(1.5\,\sigma_v/s)\,\dot{e}\,\delta t;\ \sigma_v \le 0. \tag{4.63}$$

The elastic strain components ϵ^e_{ij} are defined in Eq. (2.12) as

$$\epsilon^e_{ij} = C_{ijkl}\,\sigma_{ij}$$

where C_{ijkl} is the compliance matrix which is the inverse of stiffness matrix.

In the above equations, the stresses s, s_{ij}, σ_v, strain e^d and damage D_N are stored as state variables from previous states, and at the end of each increment, these variables will be updated as

$$\sigma_{ij}^{*} = \sigma_{ij} + \delta\sigma_{ij}, \tag{4.64}$$

$$\vdots$$

$$D_N^{*} = D_N + \delta D_N. \tag{4.65}$$

The damage equations have been implemented for numerical computation in several different forms. A simple version of the model for the uniaxial case has been implemented using MATLAB, a mathematical processing, array manipulation and graphics environment which allows for rapid confirmation of results. The complete multiaxial model has been developed in FORTRAN code and implemented as a user material specification in the ABAQUS finite element structural analysis program.

The parameters of the damage model are all calibrated from the uniaxial test results. By fitting the time-strain record of creep test on intact ice (see Fig. 4.6), the primary and secondary creep reference rates, $\dot{\epsilon}_0^d$ and $\dot{\epsilon}_0^c$ can be estimated. Then, by fitting creep test on predamaged ice (see Fig. 4.6), the damage constant, $\dot{N}_0$, and the creep enhancement parameters, β_d and β_c can be obtained. Finally the stress-strain relation predicted by the model is compared with the result of constant strain rate test, as shown in Fig. 4.7. Once the model predictions can fit the results of these three types of test, the model verification has been accomplished. All parameters used in the model are listed in Table 4.1.

Table 4.1: Parameters Used in the Damage Model

Description	Parameter	Value
Bulk Modulus	K	6667 MPa
Shear Modulus	G	3077 MPa
Primary Creep Reference Rate	$\dot{\epsilon}_0^d$	$8.8\times10^{-6}s^{-1}$ at -20°C
Creep Exponent	n	3
Poisson's Ratio	ν	0.3
Secondary Creep Ref. Rate	$\dot{\epsilon}_0^c$	$3.52\times10^{-7}s^{-1}$ at -20°C
Damage Constant	N_0	20000
Reference Stress	σ_0	1 MPa
Damage Exponent	m	3
Creep Enhancement Parameter	β_d	8
Creep Enhancement Parameter	β_c	18

Table 4.2: Test Conditions for each Ice Sample (Dorris, 1989)

σ_{33} \ $\dot{\epsilon}_{11}$	.001/sec	.01/sec
2.62 MPa	T494	T481
10 MPa	T485	T466

σ_{33} is the confining pressure; $\dot{\epsilon}_{11}$ is the strain rate.

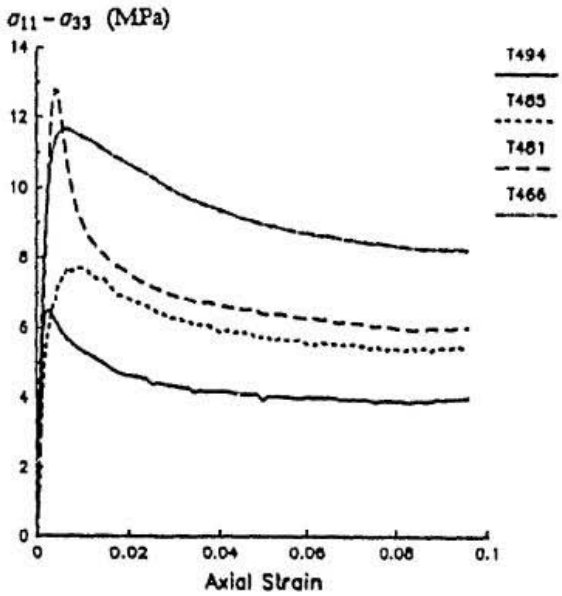

Figure 4.1: Stress versus strain curves for the four tests listed in Table 4.2 (Dorris, 1989).

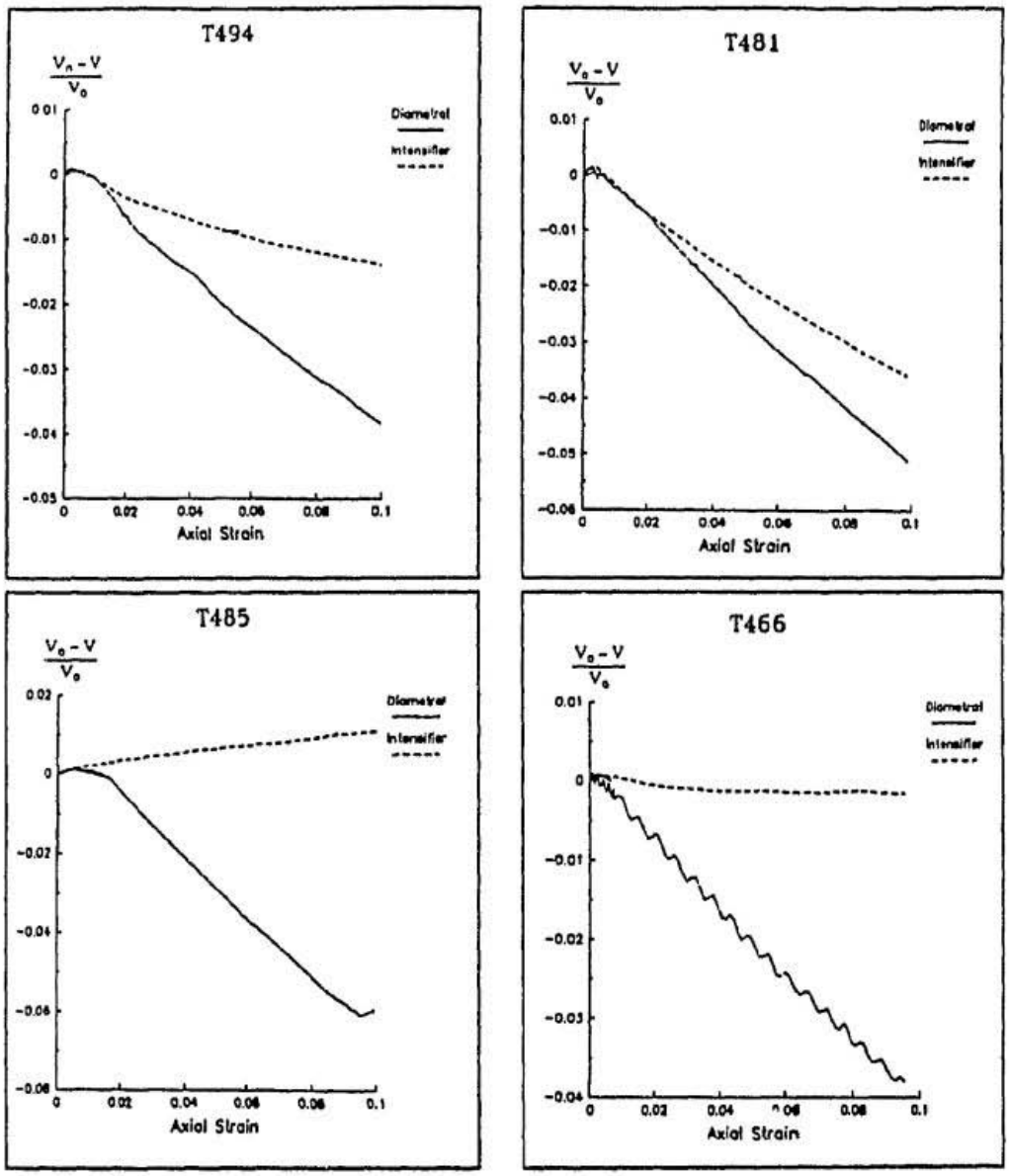

Figure 4.2: Stress versus strain curves for the four tests listed in Table 4.2 (Dorris, 1989).

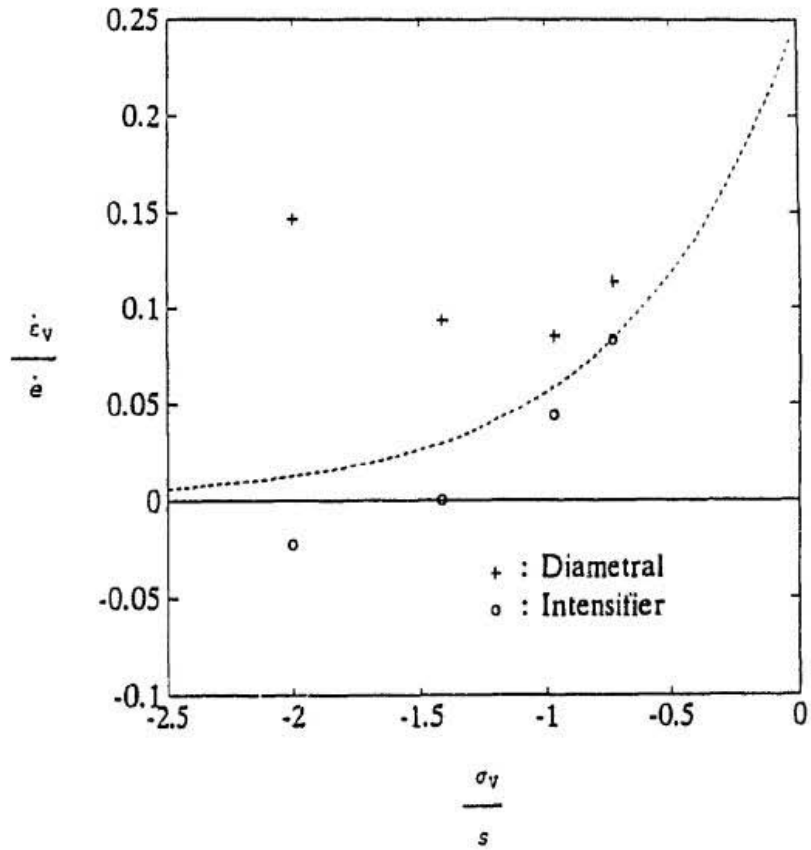

Figure 4.3: Ratio of bulk strain rate to equivalent strain rate versus ratio of bulk stress to von Mises stress. Data points were derived from Dorris (1989) Fig. 4.2 and a best fit line is shown (McKenna et al. 1990).

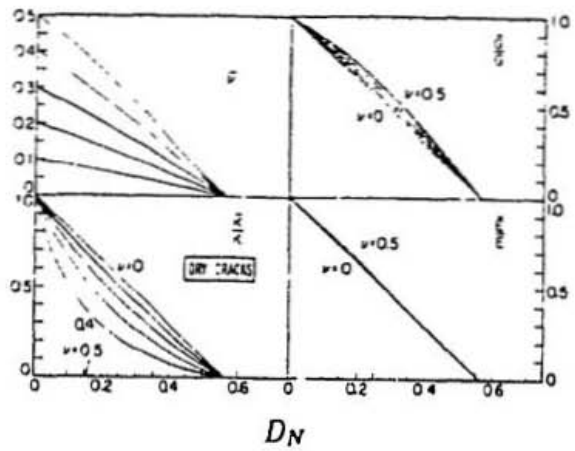

Figure 4.4: Effective moduli: dry circular cracks; G is the shear modulus; E is the Young's modulus; K is the bulk modulus and ν is the Poisson's ratio (Budiansky and O'Connell, 1976).

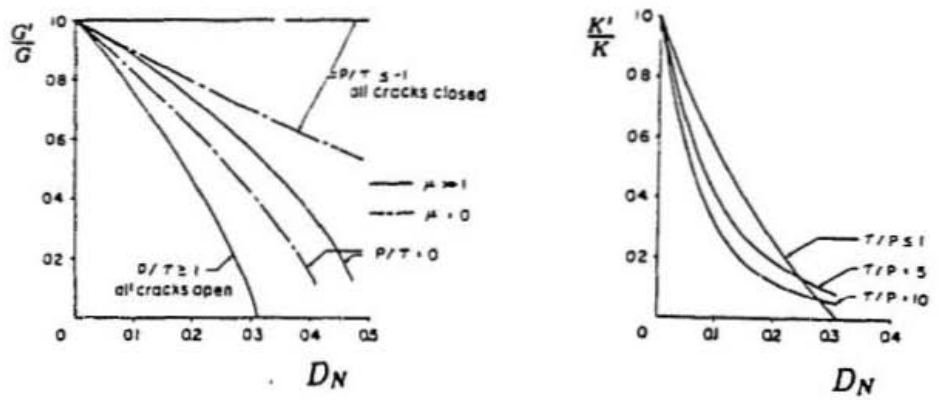

Figure 4.5: Effective moduli versus the crack-density parameter for indicated values of stress ratio, $\nu = 0.3$, where μ is the friction coefficient; P is the normal stress to the crack surface and τ is the shear stress across the crack surface (Horii and Nemat-Nasser, 1983).

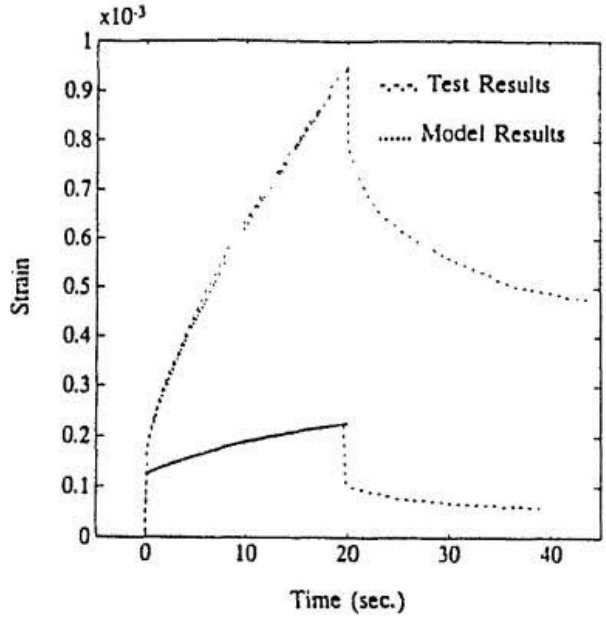

Figure 4.6: Comparison of creep test results with model results.

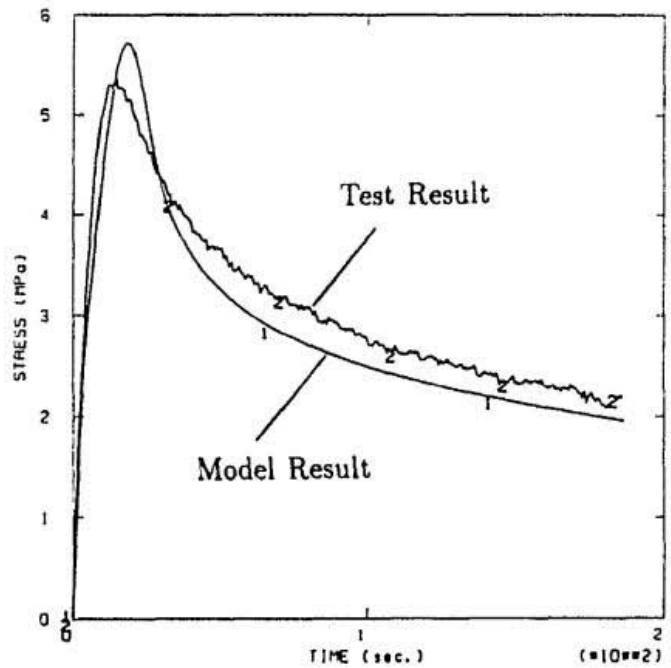

Figure 4.7: Comparison of constant strain rate test results with model results.

Chapter 5

Finite Element Modelling of Spherical Indentation Tests

The spherical indentation tests on the multiyear ice described in the previous chapters, are modelled using a symmetrical finite element model, which aid to the interpretation of the test data. In the present work the modelling results are compared to the experimental results of spherical indentation tests, NRC1 and NRC2.

5.1 The Elastic Solutions of Spherical Indentation

The theoretical elastic solutions of spherical rigid indentation problem are complex and require numerical methods to produce computational results. But the solution of total load on the indenter is much simpler, which was given by Sneddon (1964) in the form

$$P = \frac{G}{1-\nu}[(r^2 + R^2)log\frac{R+r}{R-r} - rR] \tag{5.1}$$

and

$$H = \frac{1}{2}r\,log\frac{R+r}{R-r} \tag{5.2}$$

where P is the total load on the indenter; H is the indentation depth; r is the radius of the area contacted with the indenter; R is the radius of the indenter and ν is the Poisson's ratio. This elastic solution is used to verify the finite element model.

5.2 Finite Element Model

The finite element geometry is shown in Fig. 5.1 The structure (indentation system) is assumed to be a rigid body and moving at a constant speed into the flat surface of an ice mass. The radius of the spherical surface is 1.28 m. An axisymmetrical condition has been assumed with edge a-b as the axis of symmetry (rotation). In this case half of the computation time can be saved. All the degrees of freedom of the nodes on the edges, b-c and c-d, have been constrained, since these degrees of freedom are theoretically assumed to be zero at infinity. The elastic solution of the total load on the indenter calculated from the finite element model has been compared with the theoretical elastic solution, given by Eq. (5.1) and Eq. (5.2), and is illustrated in Fig. 5.2. The reason for the numerical solution being higher than the closed form solution is the restricted boundaries in the finite element model, which are actually supposed to be free; i.e., some relative deformation should occur under the indentation load. So the difference of these two solutions increases as the total load increases. For this reason, finite element modelling of the contact problem has a size effect, i.e., before setting up the model, first one has to consider the size of the model compared with the contact length or area. Based on the author's experience, for a two dimensional problem as shown in Fig. 5.1, the mesh size in both X an Y direction should be at least five times the maximum contact

length or more. If less, lower accuracy is expected: Additionally, if the mesh is too large, more elements may be needed and much more CPU time will be consumed. Therefore, some different sizes of the model have been tested to find out the size effects, see Fig. 5.3. The present model Fig. 5.3a (see also Fig. 5.1) has a size of 3.8 m×3.8 m, the maximum contact length is about 0.3 m for test No. 1, so the mesh size is more than 12 times the maximum contact length. As shown in Fig. 5.2, the model gives reasonable results. The minimum stress near the boundaries is very small (it is supposed to be zero at infinity), only 0.1% of the maximum stress near the contact surface, while in Fig. 5.3d the minimum stress is about 4.4% of the maximum stress.

Eight-noded axisymmetrical elements have been used. There are 16 interface elements between the rigid indenter and the ice elements. The smallest elements near the interface have a size of 0.025 m ×0.050 m, and the maximum contact length is about 0.3 m for test NRC1; therefore, there are about 12 elements in contact with the indenter at the end of the run, so the interface element size is reasonable compared with the total contact length. In the ABAQUS program, multi-point constraints can be imposed such that small elements can be adjacent (linked) to larger (double-sized) elements, thereby reducing the total number of elements.

5.3 Modelling the Spherical Indentation Tests

The total load versus time records of test NRC1 and NRC2 are shown in Fig. 3.17. Following the discussions in Chapter 3, it appears that a fracture spall occurred during test NRC1 at point B, so that only section A-B of the test has been used

for modelling. A similar situation existed for test NRC2.

The same damage model described in Chapter 4, and the relevant parameters calibrated from the uniaxial tests, were implemented as a user subroutine and applied to this finite element indentation model. The modelling results of the load time history are compared to the results of test NRC1 and NRC2, in Fig. 5.4a, b, and show good agreement. The periodic fluctuation in load of the model result is associated with the discretization of the finite elements in the contact problem. It is worth comparing the results shown in Fig. 5.4a with those in Fig. 5.2. These load-time history curves were all obtained from the same finite element model under same loading and boundary conditions (i.e., the same indentation speed, penetration and boundary constraints), except that in Fig. 5.2, the ice was assumed to be a purely elastic material with same Young's modulus as the multiyear ice (8000 MPa), and in Fig. 5.4a, ice damage model has been implemented. It can be seen from Fig. 5.2 that the total load on the indenter is about 30 MN, as much as 10 times higher than that in Fig. 5.4a. This means that damage and creeping in the ice have significantly reduced its strength, and the ice is no longer behaving as a purely elastic material.

Following the discussions in Chapter 3, the crushed layer thickness of the spherical indentation test is usually smaller in the center or high pressure zones and increases with distance away from these zones. The damage distributions of the two tests are plotted in Fig. 5.5. At the end of each simulation, damage contour levels 8 to 10 ($D_N = 0.4$ to 0.5) cover most of the area adjacent to the contact face. The figures also show that there is less damage in the center area due to high confining pressure and more damage at the edge of the interface where concentrated

shear stresses are high and confinement is low. This area can be characterized, to a certain degree, as the crushed layer.

Tensile zones with stresses between 1 to 2 MPa have also been found in the simulations, as shown in Fig. 5.6. These tensile zones can be related to macrocrack development and spalling, i.e., a macrocrack could be triggered due to the linkage of the microcracks or the development of a small flaw in these tensile zones. These may become a macrocrack and possibly grow towards the ice surface, developing a fracture spall. Based on the work of Schulson (1987, 1989), the tensile strength or critical tensile stress for crack nucleation of granular freshwater ice is about 0.5 to 2 MPa, depending on the grain size and the loading rate. The data were obtained from relatively bubble-free ice at strain rates of $10^{-7}\,s^{-1}$ and $10^{-3}\,s^{-1}$. This suggests that the development of a tensile crack is not necessarily due to the existence of a microcrack or flaw. It could be the result of grain boundary sliding or the stress concentration at grain boundaries due to the elastic anisotropy of ice. In any case, the existence of damage or flaws in the ice will reduce its strength, which in return will make it easier for the growth of macrocracks.

Friction between ice and indenter has been ignored. This would be reasonable if pressure melting occurs. It might not be an accurate assumption in all cases.

Calculated interface pressures for test NRC1 are of the same order as measured local pressures (see Fig. 5.7). The initial contact pressures are as high as 20 MPa, which is very close to the test results, and then reduced as damage progressed into the ice, but the pressure is always higher in the center area and its distribution is approximately parabolic.

5.4 Equivalent Viscosity of Damaged Ice

As discussed in Chapter 4, the creep strains of intact ice in both the Kelvin unit and the Maxwell unit are defined to follow power-law relations with stress, and the viscosity coefficients are expressed in Eq. (4.19) and Eq. (4.20), i.e.

$$\mu_k = (s/\dot{\epsilon}_0^d)(\sigma_0/s^d)^n, \text{ and}$$

$$\mu_m = (s/\dot{\epsilon}_0^c)(\sigma_0/s)^n.$$

The creep enhancement factors due to damage are given in Eq. (4.49) and Eq. (4.50) as $\exp(\beta_d D_N)$ and $\exp(\beta_c D_N)$, respectively. So the viscosity coefficients of damaged ice can be expressed as

$$\mu_k' = (s/\dot{\epsilon}_0^d)(\sigma_0/s^d)^n \exp(-\beta_d D_N) \text{ and} \tag{5.3}$$

$$\mu_m' = (s/\dot{\epsilon}_0^c)(\sigma_0/s)^n \exp(-\beta_c D_N). \tag{5.4}$$

The equivalent viscosity coefficient of damaged ice is then defined as a function of von Mises stress and damage in the form

$$\mu = \frac{\mu_k' \mu_m'}{\mu_k' + \mu_m'}. \tag{5.5}$$

Fig. 5.8 shows the relation of viscosity with stress and damage. The viscosity of water and the equivalent viscosity of intact ice are also included for comparison, since the viscosity of damaged ice should fall within this range for pressures greater than 1 MPa.

As discussed in Jordaan and Timco (1988) and Finn et al. (1989), the viscosity of the crushed ice is calculated about 0.0009 to 1.0 MPa.s in the speed range of 160

mm/s to 2.5 mm/s. In general, higher speed gives lower viscosity. The progression and distribution of calculated equivalent viscosity adjacent to the interface are shown in Fig. 5.9 and Fig. 5.10, respectively. It can be seen that the modelled viscosities are higher than the range mentioned above. It is necessary to have more experiments and good measurements on the actual viscosities, so that better understanding and modelling of the crushed ice can be achieved.

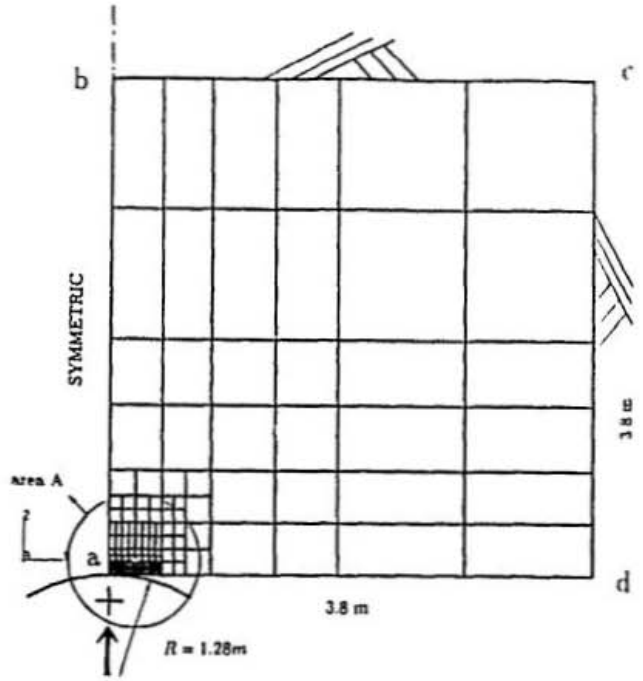

Figure 5.1: Finite element mesh for spherical indentation tests.

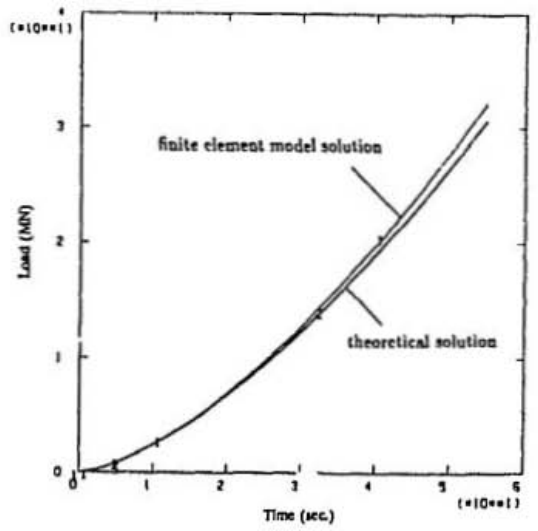

Figure 5.2: Comparison of theoretical elastic solution of spherical indentation with finite element solution.

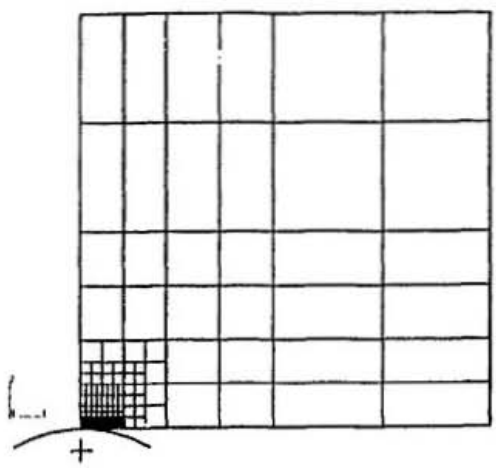

(a) 3.8 m × 3.8 m

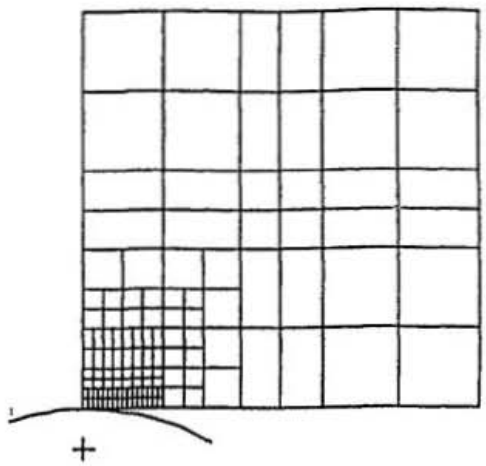

(b) 2 m × 2 m

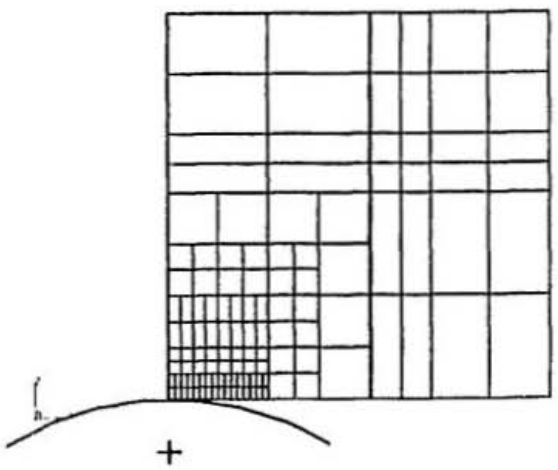

(c) 1.5 m × 1.5 m

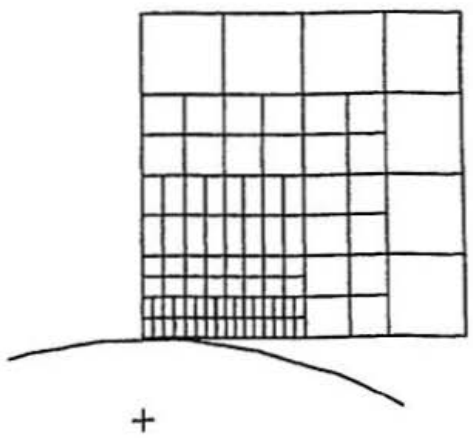

(d) 0.8 m × 0.8 m

Figure 5.3: Four different mesh sizes have been tested for comparisons.

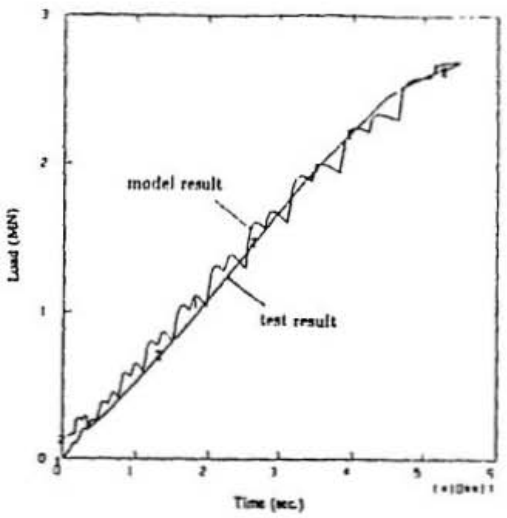

(a)

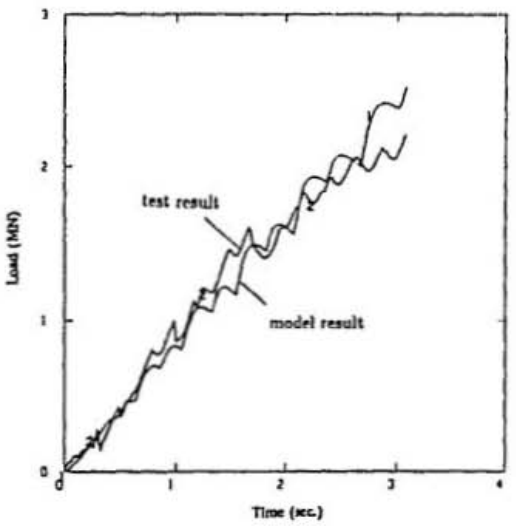

(b)

Figure 5.4: The total load vs. time histories: model results and test results; (a) test NRC1; (b) test NRC2.

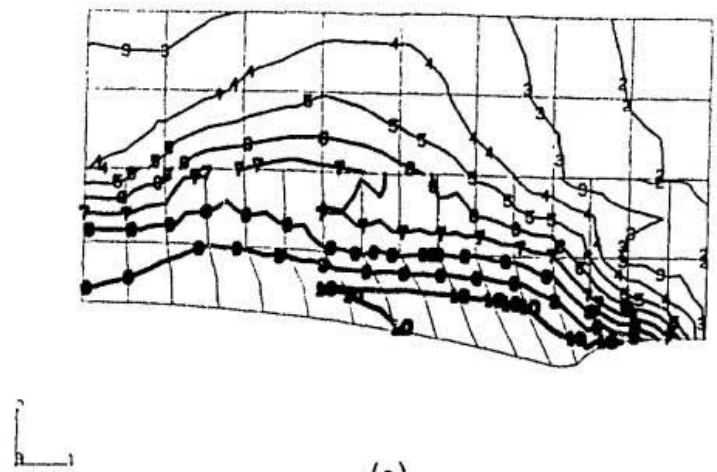

(a)

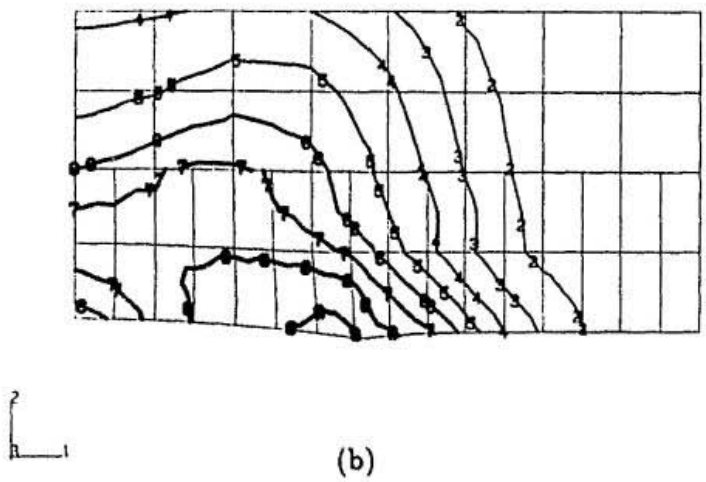

(b)

Figure 5.5: Distributions of damage, D_N, in the ice adjacent to the indenter (area A, see Fig. 5.1). $D_N = 0$ for contour level 1; $D_N = 0.5$ for contour level 10, the increment of D_N for each contour level is 0.05. (a) test NRC1; (b) test NRC2.

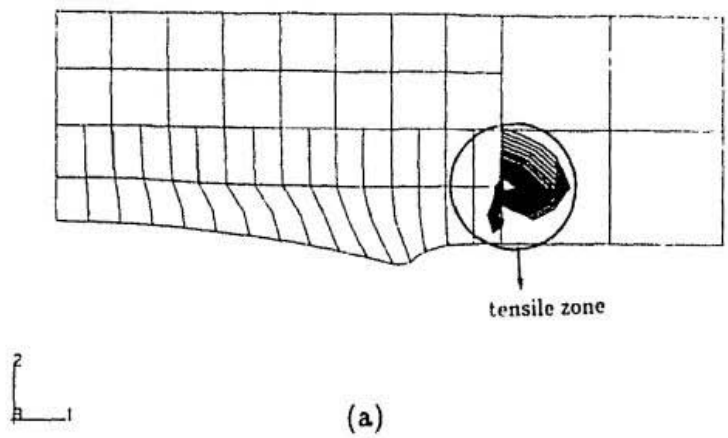

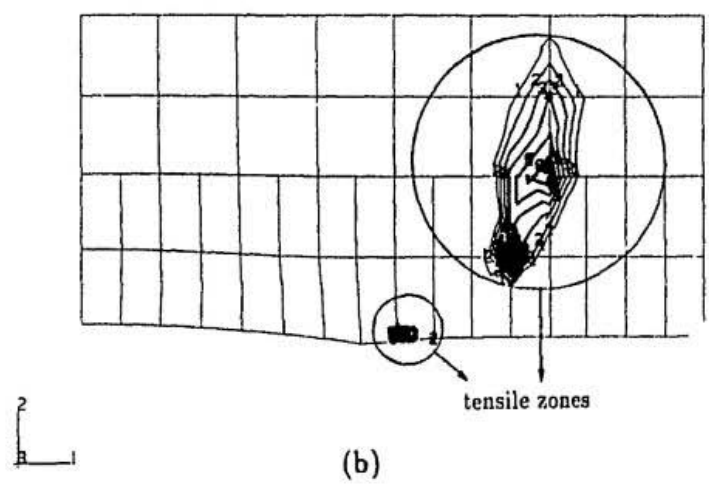

Figure 5.6: Distributions of maximum principal stress between 1 MPa and 2 MPa near the contact face: (a) test NRC1; (b) test NRC2.

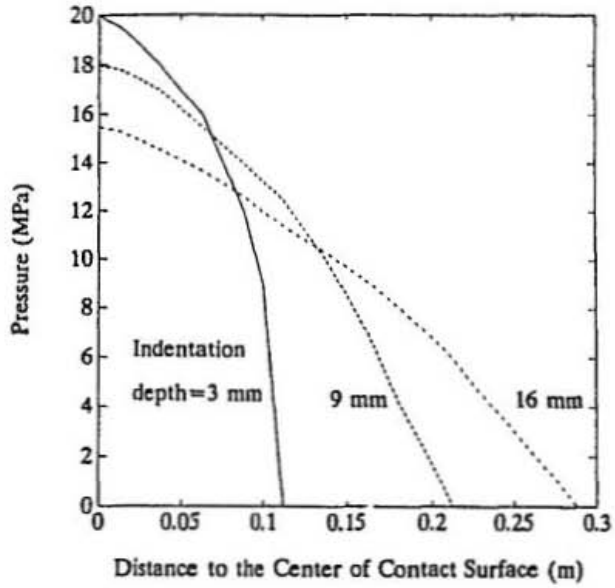

Figure 5.7: Calculated pressure distributions for test NRC1 on the contact face.

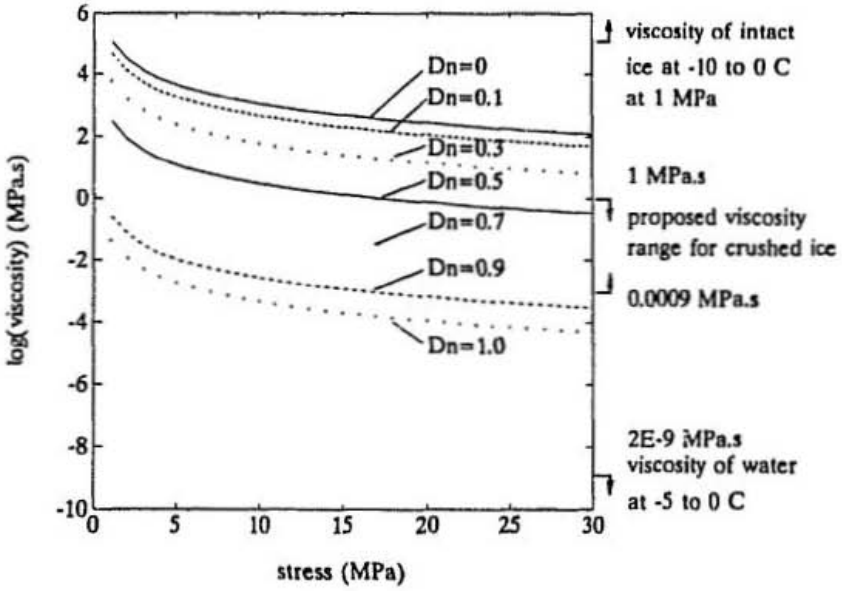

Figure 5.8: Modelled equivalent viscosity of ice as a function of applied shear stress and damage state.

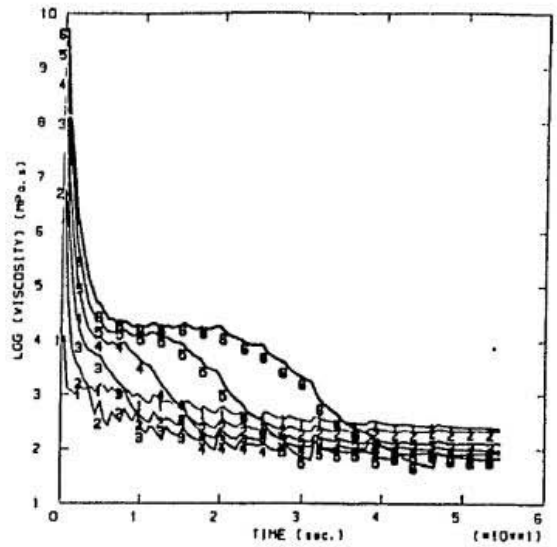

(a)

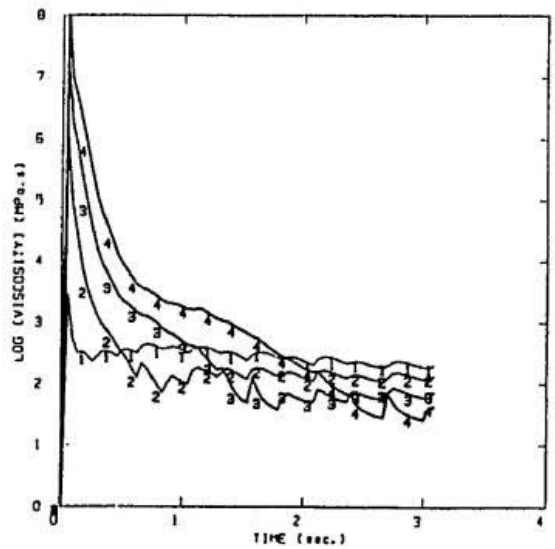

(b)

Figure 5.9: Progression of equivalent viscosity adjacent to the contact face: (a) test NRC1; (b) test NRC2.

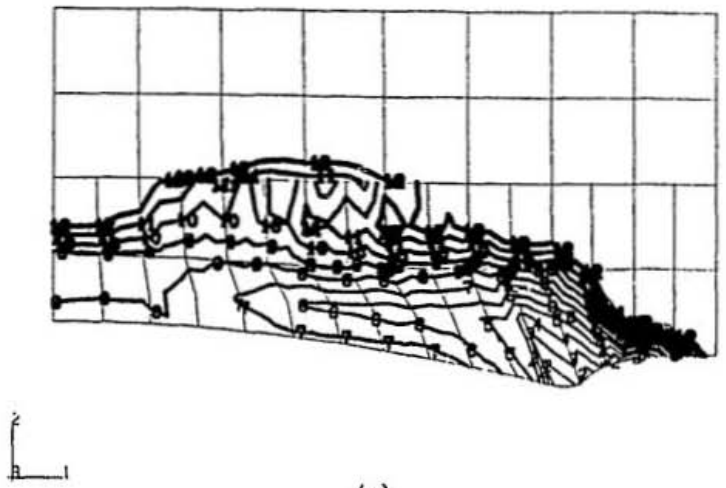

(a)

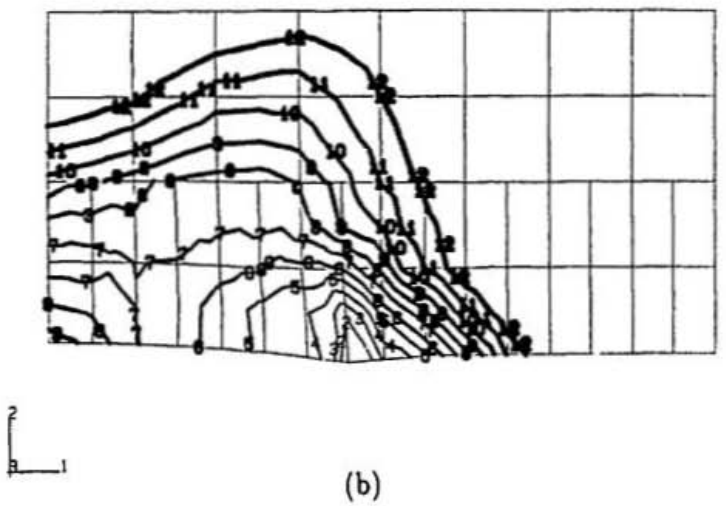

(b)

Figure 5.10: Distributions of equivalent viscosity between 20 MPa.s (contour level 1) and 1000 MPa.s (contour level 10) adjacent to the contact face: (a) test NRC1; (b) test NRC2.

Chapter 6

Conclusions

Uniaxial laboratory tests on the multiyear ice, as well as medium-scale ice indentation experiments on Hobson's Choice Ice Island (1989) have been described, together with the development and implementation of an ice damage model. The study is a comprehensive examination of the role of the damage process in ice, as well as the influence of damage on mechanical properties of ice. Investigations on the creep tests on both intact and predamaged ice have shown clear evidence of an enhancement of the creep strain due to cracks and damage.

The model predictions of the strain-stress relations for uniaxial tests, as well as the total load versus time histories for the indentation tests show good agreement with the measured results. Both the magnitude and distribution of the contact pressure calculated from the model are realistic. The tensile fracture or spalling is not included in the present work, but it may be able to predict, to a certain degree, when and where a spall might have occurred in the light of the calculation of the maximum principal stress. Further study on modelling of fractures and spalls is recommended. In a separate work, fracture and damage analyses of production of discrete ice pieces have been carried out by introducing a small flaw, and predicting

the flaw growth time and direction (see Xiao and Jordaan, 1991).

Based on the analysis of the experimental results and the finite elements simulations detailed in this work, some general conclusions can be made as follows:

1. The recoverable strain, i.e., elastic strain plus delayed elastic strain, is about 10% of the total strain or less, for the constant strain rate tests, after the stress reaches a plateau.

2. The presence of cracks and damage significantly enhances the creep responses (delayed elastic strain plus secondary strain). The creep strain of predamaged ice is as much as 5 to 10 times larger than that of intact ice.

3. The idealized ice damage model, consisting of combination of a Maxwell unit and a Kelvin unit with a nonlinear dashpot in each unit, has been shown to be appropriate for describing the ice behaviour under certain loading conditions, such as proportional compressive loading.

4. Due to the domination of creep strain for a high degree of damage, the elastic strain is relatively small, so the specifications of elastic moduli in the model are not critical, while the determination of viscosities becomes significant. This is influenced by the existence of damage, confining pressure (pressure melting) and loading rate (internal friction). More accurate experimental results of ice viscosities are needed.

5. This finite element model can provide realistic results on load-time histories; damage distribution and progression; contact pressure distribution and progression and viscosity progression. The estimation of crushed ice layer

thickness can be made possible when more measurements on the distribution of damage are obtained.

References

Ashby, M.F. and Duval, P., 1985. The Creep of Polycrystalline Ice, Cold Regions Science and Technology, Vol. 11, pp. 285-300.

Bezukhov, N.I., 1953. Theory of Elasticity and Plasticity. Gostekhizdat, Moskva.

Budiansky, B. and O'Connell, R.J. 1976. Elastic Moduli of a Cracked Solid, International Journal of Solids and Structures, Vol.12, pp.81-97.

Cammaert, A.B. and Muggeridge, D.B., 1988. Ice Interaction with Offshore Structures. Van Nostrand Reinhold, New York.

Cole, D.M., 1986. Effect of Grain Size on the Internal Fracturing of Polycrystalline Ice, CRREL Report 86-5.

Cole, D.M., 1988. Crack Nucleation in Polycrystalline Ice. Cold Regions Science and Technology, Vol. 15, pp. 79-87.

Cole, D.M., 1989. Microfracture and the Compressive Failure of Polycrystalline Ice. Proceedings IUTAM/IAHR Symposium on Ice-Structure Interaction, St. John's, Newfoundland, Canada, pp. 231-250.

Cormeau, A., Jordaan, I. J., and Maes, M., 1986. Development of a model for progressive damage in ice. Det norske Veritas (Canada) Ltd. Calgary, Alberta.

Currier, J.H. and Schulson, E.M., 1982. The Tensile Strength of Ice as a Function of Grain Size. Acta Metallurgica. Vol. 30, pp. 1511-1514.

Dorris, J.F. 1989. A Plasticity Model for the Crushing of Ice, Proceedings IUTAM/IAHR Symposium on Ice-Structure Interaction, St. John's, Newfoundland, Canada, pp. 311-338.

Finn, D.W., Jordaan, I.J., Singh, S.K. and Spencer, P., 1989. Flow of Crushed Ice: Physical and Mechanical Properties and Behavior, Ocean Engineering Research Centre, Memorial University of Newfoundland, St. John's, NF (proprietary).

Finn, D., 1991. M. Eng. Thesis, Memorial University of Newfoundland.

Frederking, R.M.W. et al., 1990a. Field Tests on Ice Indentation at Medium Scale, Ice Island, April 1989. National Research Council of Canada Report CR 5866.1.

Frederking, R.M.W., Jordaan, I.J. and McCallum, J.S. 1990b. Field Tests of Ice Indentation at Medium Scale, Hobson's Choice Ice Island, Proc. 10th International IAHR Symposium on Ice, Espoo, Finland, Vol. 2, pp. 931-944.

Gagnon, R.E. and Molgaard, J., 1990. Evidence for Pressure Melting and Heat Generation by Viscous Flow of Liquid in Indentation and Impact Experiments on Ice. Presented at the IGS Symposium on Ice-Ocean Dynamics and Mechanics, Dartmouth College, Hanover, New Hampshire.

Gagnon, R.E. and Sinha,N.K., 1991. Energy Dissipation Through Melting in Large Scale Indentation Experiments on Multi-Year Sea Ice, Proceedings, OMAE, Vol. IV, pp. 157-161.

GEOTECH (GEOTECHnical resources Ltd.), 1985. Medium Scale Iceberg Impact Simulation Test Program, report prepared for Mobil Oil Canada Ltd..

Glen, J.W., 1955. The Creep of Polycrystalline Ice, Proceedings Royal Society of London, Piccadilly, London, W., Ser. A, Vol. 228, pp. 519-538

Gold, L.M., 1970. Process of Failure in Ice. Canadian Geotechnical Journal, Vol. 7, pp. 405-413.

Gold, L.M., 1972. The Failure Process in Columnar-grained Ice, Technical Paper No. 369, Division of Building Research, NRC.

Hallam, S.D., 1986. The Role of Fracture in Limiting Ice Force, Proceedings of IAHR Ice Symposium, Iowa City, Iowa, pp. 287-319.

Hallam, S.D., Duval, P. and Ashby, M.F., 1987. A study of Cracks in Polycrystalline Ice Under Uniaxial Compression, J. de Physique, Tome 48, pp. C1-303-311.

Horii, H. and Nemat-Nasser, S. 1983. Overall Moduli of Solids with Microcracks: Load-Induced Anisotropy, Journal of Mechanics and Physics of Solids, Vol.31, No.2, pp.155-171.

Jordaan, I.J. and Timco, G.W., 1988. Dynamics of the Ice Crushing Process, Journal of Glaciology, Vol. 34, No. 118, pp. 318-326

Jordaan, I.J., Maes, M. and Nadreau, J.P., 1988. The Crushing and Clearing of Ice in Fast Spherical Indentation Tests, OMAE '88, Proceedings of the Seventh International Offshore Mechanics and Arctic Engineering Symposium, Vol. 4, New York, American Society of Mechanical Engineers, pp. 111-116

Jordaan, I.J. and McKenna, R.F., 1988a. Modelling of Progressive Damage in Ice, IAHR Symposium on Ice, Sapporo, Japan, August, Proceedings Vol. II, pp. 585-624

Jordaan, I.J. and McKenna, R.F. 1988b. Constitutive Relations for Creep of Ice, Proceedings International Association for Hydraulic Research (IAHR) Ice Symposium, Sapporo, Japan, Vol.3, pp.47-58.

Jordaan, I.J. and McKenna, R.F. 1989. Processes of Deformation and Fracture of Ice in Compression, Proceedings IUTAM/IAHR Symposium on Ice-Structure Interaction, St. John's, Newfoundland, Canada, pp. 283-310.

Jordaan, I.J., Stone, B.M., McKenna, R.F. and Fuglem, M.K. 1990a. Effect of Microcracking on the Deformation of Ice, Proceedings of the 43rd Canadian Geotechnical Conference, Quebec, pp. 387-393.

Jordaan, I.J., McKenna, R.F., Duthinh, D., Fuglem, M.K, Kennedy, K.P., Maes, M.A. and Marshall, A., 1990b. Development of New Ice Load Models, report for Canada Oil and Gas Lands Administration (COGLA) by (C-CORE), Memorial University, St, John's, NF.

Kachanov, L.M., 1958. On the Creep Rupture Time. Izv. AN SSSR, Ofd. Tekhn. Nauk., No. 8, pp. 26-31.

Kachanov, L.M., 1986. Introduction to Continuum Damage Mechanics. Martinus Nijhoff Publishers.

Kalifa, P., Duval, P. and Ricard, M., 1989. Crack Nucleation in Polycrystalline Ice Under Compressive States. Proceedings, OMAE, A.S.M.E., Vol. 4, pp 13-21.

Karr, D. G., 1985. A damage mechanics model for uniaxial deformation of ice. OMAE'85, Vol. 2, pp. 227-233.

Karr, D.G. and Choi, K., 1989. A Three-Dimensional Constitutive Damage Model for Polycrystalline Ice, Mechanics of Materials, Vol. 8, pp. 55-66.

Kennedy, K.P., 1990. M. Eng. Thesis, Memorial University of Newfoundland.

Krajcinovic, D., and Fonseka, G. U., 1981. The continuous damage theory of brittle materials, Journal of Applied Mechanics, Vol. 48, pp. 809-824.

Krajcinovic, D., 1983. Constitutive equations for damage materials, Journal of Applied Mechanics, Vol. 50, pp. 355-360.

Leckie, F.A., 1978. The Constitutive Equations of Continuum Creep Damage Mechanics. Phil. Transactions of the Royal Society, London, Series A, 288, pp. 27-47.

McKenna, R.F., Meyssonnier, J. and Jordaan, I.J., 1989. Peak Pressures from a Damage Model for Ice in Compression, Proceedings of the Eighth International Conference on Offshore Mechanics and Arctic Engineering, the Hague, Netherlands, Vol. IV, pp.67-73.

McKenna, R.F., Jordaan, I.J. and Xiao, J., 1990. Analysis of Damage and Energy Flow in the Crushed Layer during Rapid Ice Loading, Proceedings of IAHR Symposium on Ice, Espoo, Finland, Vol. 3, pp. 231-245.

Mellor, M. and Cole, D. M., 1982. Deformation and Failure of Ice under Constant Strain-Rate, Cold Regions Science and Technology, Vol. 5, pp. 201-219.

Mellor, M., 1983. Mechanical Behaviour of Sea Ice, U.S. Army Cold Region Research and Engineering Lab,Hanover, CRREL Report 83-1.

Michel, B., 1979. Ice Mechanics, Universite Laval Press.

Ohno, N., Murakami, S. and Ueno, T., 1985. A Constitutive Model of Creep Describing Creep Recovery and Material Softening Caused by Stress Reversals, Journal of Engineering Materials and Technology, Vol. 107, pp. 1-6.

Pounder, E.R., 1965. The Physics of Ice. Pergamon Press, London.

Resende, L. and Martin, J.B., 1983. Damage Constitutive Model for Geotechnical Applications. Technical report No. 44, Dec. 83.

Resende, L. and Martin, J.B., 1984. A Progressive Damage Continuum Model for Granular Materials. Computer Methods in Applied Mech. and Eng. 42, 1-18 North Holland.

Sanderson, T.J.O. 1988. Ice Mechanics-Risks to Offshore Structures, Graham and Trotman.

Schapery, R.A., 1981. On Viscoelastic Deformation and Failure Behaviour of Composite Materials with Distributed Flaws. Advances in Aerospace Structures and Materials. The American Society of Mechanical Engineers, pp. 5-20.

Schapery, R. A., 1984. Correspondence Principles and a Generalized J Integral for Large Deformation and Fracture analysis of Viscoelastic Media. Int. Journal of Fracture, Vol. 25, pp. 195-223.

Schapery, R. A., 1988. A theory of mechanical behaviour of elastic media with growing damage and other changes in structure, Mechanics and Materials Center, Texas A and M Univ., College Station, Texas, Report No. MM. 5762-88-1.

Schulson, E.M. and Cannon, N.P., 1984. The Effect of Grain Size on the Compressive Strength of Ice. IAHR Ice Symp. Hamburg. pp. 24-38.

Schulson, E.M., 1987. The Fracture of Ice Ih, J. de Physique, 48: C1-207-220.

Schulson, E.M., 1989. The Tensile and Compressive Fracture of Ice, Proceedings IUTAM/IAHR Symposium on Ice-Structure Interaction, St. John's, Newfoundland, Canada, pp. 165-184.

Schulson, E.M., Hoxie, S.G. and Nixon, W.A., 1989. The Tensile Strength of Cracked Ice. Phil. Mag., Vol. 59, pp. 303-311.

Schwarz, J., and Weeks,W.,F., 1977. Engineering Properties of Sea Ice, Journal of Glaciology, Vol 19, No. 81, pp 499-531.

Seng-Kiong, T. and Shyam Sunder, S., 1985. Constitutive Modelling of Sea Ice with Applications to Indentation Problems, CSEOE Research Report No. 3, MIT, Cambridge, Massachusetts.

Shyam Sunder, S. and Wu, M.S. 1990. Crack Nucleation due to Elastic Anisotropy in Polycrystalline Ice, Cold Regions Science and Technology.

Sinha, N.K., 1978. Rheology of Columnar-Grained Ice, Experimental Mechanics, Vol. 18, No. 12, pp. 464-470.

Sinha, N.K., 1981. Deformation Behaviour of Ice-Like Materials in Engineering Applications, Proc. International Symposium on Mechanical Behaviour of Structured Media, Ottawa, pp. 419-430.

Sinha, N.K., 1982. Delayed Elastic Strain Criterion for First Cracks in Ice, Proc. of the Symposium on Deformation and Failure of Granular Materials, pp. 323-330. Rotterdam: Balkema.

Sinha, N.K., 1983. Creep Model of Ice For Monotonically Increasing Stress, Cold Regions Science and Technology, Amsterdam, Vol. 8, No. 1, pp. 25-33.

Sinha, N.K. 1984. Intercrystalline Cracking, Grain-Boundary Sliding, and Delayed Elasticity at High Temperatures, Journal of Material Science, London, Vol.19, pp. 359-376.

Sinha, N.K., 1988. Crack-Enhanced Creep in Polycrystalline Material: Strain-Rate Sensitive Strength and Deformation of Ice, J. of Materials Science, Vol. 23, No. 12, pp. 4415-4428.

Sinha, N.K., 1989a. Elasticity of Natural Types of Polycrystalline Ice. Cold Regions Science and Technology, Vol. 17, pp. 127-135.

Sinha, N.K. 1989b. Kinetics of Microcracking and Dilatation in Polycrystalline Ice, Proceedings IUTAM/IAHR Symposium on Ice-Structure Interaction, St. John's, Newfoundland, Canada, pp. 69-87.

Sinha, N.K. 1990. In Situ Multiyear Sea Ice Strength and Deformation using NRCC Borehole Indentor. To be presented at OMAE, 1991.

Sjölind, S.G., 1987. A Constitutive Model for Ice as a Damaging Visco-Elastic Material. Cold Regions Science and Technology, No. 41, pp. 247-262.

Sneddon, I.N., 1964. Technical Report AFOSR 64-1989, North Carolina State University.

Stone, B.M., Jordaan, I.J., Jones, S.J. and McKenna, R.F. 1989. Damage of Isotropic Polycrystalline Ice Under Moderate Confining Pressures, Proceedings of the 10th International Conference on Port and Ocean Engineering under Arctic Conditions, Lula, Sweden, Vol.1, pp.408-419.

Timco, G.W., 1986. Indentation and Penetration of Edge-Loaded Freshwater Ice Sheets in the Brittle Range, Fifth OMAE Symposium, Proceedings Vol. IV, pp. 444-452

Timco, G.W. and Jordaan, I.J., 1988. Time-Series Variations in Ice Crushing, POAC '87, Proceedings of the 9th International Conference on Port and Ocean Engineering Under Arctic Conditions, Fairbanks, Alaska, pp. 13-20.

Tomin, M., Cheung, M., Jordaan, I.J. and Cormeau, A., 1986. Analysis of Failure Modes and Damage Processes of Freshwater Ice in Indentation Tests. Proc. of 5th OMAE Symp., Tokyo, Vol. IV, pp. 453-460.

Wang, Y.S., 1979a. Sea Ice Properties. Technical Seminar. Exxon Company, USA.

Wang, Y.S., 1979b. Crystallographic Studies and Strength tests of Field Ice in the Alaskan Beaufort Sea. In POAC 79, pp. 651-655.

Wang, Y.S., 1981. Uniaxial Compression Testing of Arctic Sea Ice. Proc. of 6th POAC, Vol. 1, pp. 346-355.

Weeks, W.F. and Assur, A., 1967. The Mechanical Properties of Sea Ice. CRREL Monograph II-C3.

Weertman,J., 1969. Effects of Cracks on Creep Rate, Transactions Quarterly, Transactions of the ASM, Vol. 62, No. 2, pp. 502-511.

Xiao, J. and Jordaan, I.J., 1991. Modelling of Fracture and Production of Discrete Ice Pieces, a report prepared for Canada Oil and Gas Lands Administration (COGLA).

Xiao, J., Jordaan,I.J., McKenna, R.F. and Frederking, R.M.W., 1991. Finite Element Modelling of Spherical Indentation Tests on Ice. Proc. of the 11th International Conference on Port and Ocean Engineering under Arctic Conditions, Sept., 1991, St. John's, NFLD.

Życzkowski, M. 1981. Combined Loadings in the Theory of Plasticity, PWN-Polish Scientific Publishers, Warszawa.

Appendix A

The Relationship between von Mises Stress and Equivalent Strain

In elasticity, Hooke's law can be expressed as

$$\sigma_{ij} = 3\lambda\epsilon_v\delta_{ij} + 2G\epsilon_{ij} \tag{A.1}$$

where λ is Lamé's constant:

$$\lambda = \frac{\nu E}{(1+\nu)(1-2\nu)}. \tag{A.2}$$

When the three stress components, σ_{ii}, are equal to the principal values, i.e.

$$\begin{aligned} \sigma_{11} &= \sigma_1 \\ \sigma_{22} &= \sigma_2 \\ \sigma_{33} &= \sigma_3, \end{aligned} \tag{A.3}$$

then the three strain components are also in the principal directions and $\sigma_{ij} = 0$, $\epsilon_{ij} = 0$ $(i \neq j)$. So the above Eq. (A.1) can be written as

$$\sigma_i = 3\lambda\epsilon_v + 2G\epsilon_i, \tag{A.4}$$

where σ_i and ϵ_i are principal stresses and strains, respectively. Then it is found that

$$\begin{aligned} \sigma_1 - \sigma_2 &= 2G(\epsilon_1 - \epsilon_2) \\ \sigma_2 - \sigma_3 &= 2G(\epsilon_2 - \epsilon_3) \\ \sigma_3 - \sigma_1 &= 2G(\epsilon_3 - \epsilon_1). \end{aligned} \tag{A.5}$$

So

$$[(\sigma_1-\sigma_2)^2+(\sigma_2-\sigma_3)^2+(\sigma_3-\sigma_1)^2]^{1/2} = 2G[(\epsilon_1-\epsilon_2)^2+(\epsilon_2-\epsilon_3)^2+(\epsilon_3-\epsilon_1)^2]^{1/2}. \tag{A.6}$$

The definition of von Mises stress is given by

$$\begin{aligned} s &= (\frac{3}{2}s_{ij}s_{ij})^{1/2} \\ &= \frac{1}{\sqrt{2}}[(\sigma_1 - \sigma_2)^2 + (\sigma_2 - \sigma_3)^2 + (\sigma_3 - \sigma_1)^2]^{1/2}. \end{aligned} \tag{A.7}$$

Thus

$$\begin{aligned} s &= \frac{2G}{\sqrt{2}}[(\epsilon_1 - \epsilon_2)^2 + (\epsilon_2 - \epsilon_3)^2 + (\epsilon_3 - \epsilon_1)^2]^{1/2} \\ &= \frac{E}{\sqrt{2}(1-\nu)}[(\epsilon_1 - \epsilon_2)^2 + (\epsilon_2 - \epsilon_3)^2 + (\epsilon_3 - \epsilon_1)^2]^{1/2}. \end{aligned} \tag{A.8}$$

The strain intensity or effective strain ϵ_e is defined as (Bezukhov, 1953)

$$\epsilon_e = \frac{1}{\sqrt{2}(1-\nu)}[(\epsilon_1 - \epsilon_2)^2 + (\epsilon_2 - \epsilon_3)^2 + (\epsilon_3 - \epsilon_1)^2]^{1/2}, \tag{A.9}$$

for compressible as well as incompressible materials in the elastic range. So

$$s = E\epsilon_e \tag{A.10}$$

The equivalent strain e is defined as

$$\begin{aligned} e &= (\frac{2}{3}e_{ij}e_{ij})^{1/2} \\ &= \frac{\sqrt{2}}{3}[(\epsilon_1-\epsilon_2)^2+(\epsilon_2-\epsilon_3)^2+(\epsilon_3-\epsilon_1)^2]^{1/2}. \end{aligned} \tag{A.11}$$

Comparing e to ϵ_e, it is found that

$$\epsilon_e = \frac{3}{2(1+\nu)}e. \tag{A.12}$$

So, when $\nu = 0.5$, for incompressible materials, $\epsilon_e = e$, and

$$\begin{aligned} s &= \frac{3E}{2(1+\nu)}e \\ &= 3Ge. \end{aligned} \tag{A.13}$$

Since

$$s_{ij} = 2Ge_{ij}. \tag{A.14}$$

So the relationship between von Mises stress and equivalent strain is expressed as

$$e_{ij} = \frac{3}{2}\frac{e}{s}s_{ij}. \tag{A.15}$$